Fall 1-8-2021

Sub-Epidemic Generalized Logistic-Growth Model Performance for Influenza Season in the United States, October 2015–April 2019

Hannah Fast

ABSTRACT

SUB-EPIDEMIC GENERALIZED LOGISTIC-GROWTH MODEL PERFORMANCE FOR INFLUENZA SEASON IN THE UNITED STATES, OCTOBER 2015–APRIL 2019

by

Hannah E. Fast

15 December 2020

INTRODUCTION: The public health response to an emerging infectious disease epidemic is based on risk assessments that predict the severity of the health threat. Although infectious disease surveillance data is often limited in scope, mathematical models can provide meaningful information about epidemic growth dynamics to inform development of public health interventions.

AIM: This investigation aims to validate application of a sub-epidemic version of the generalized logistic-growth model (GLM) to a delineated period of epidemic growth representing the influenza season, using national surveillance data for incidence of influenza-like illness (ILI) in the United States.

METHODS: Surveillance data for ILI case counts were obtained from the Centers for Disease Control and Prevention (CDC) website, FluView. GLM models with one, two, and three sub-epidemics were fit to four epidemic growth periods across four years, each containing 30 weekly ILI incidence counts. Parameter estimates were obtained through nonlinear least squares curve-fitting and sub-epidemic curves were aggregated into the best fit model. Model performance was evaluated using calculation of performance metrics, bootstrapping, and visual analysis.

RESULTS: Model performance consistently improved across all four seasons as the number of sub-epidemics incorporated into the GLM increased (n=1 to n=3). The parameter and sub-epidemic estimates provided information about the growth dynamics of the epidemic period, identifying trends specific to each season.

DISCUSSION: The sub-epidemic GLM provides useful results about epidemic dynamics using national case count data. In addition, while logistic growth models are often applied to discrete outbreaks, the results of this investigation support application of the model to periods of epidemic growth within seasonal trends as well. The findings support the continued use of this model for academic and other public health application.

SUB-EPIDEMIC GENERALIZED LOGISTIC-GROWTH MODEL PERFORMANCE FOR INFLUENZA SEASON IN THE UNITED STATES, OCTOBER 2015–APRIL 2019

by

HANNAH E. FAST

B.A., BETHEL UNIVERSITY

B.S., BETHEL UNIVERSITY

A Thesis Submitted to the Graduate Faculty

of Georgia State University in Partial Fulfillment

of the

Requirements for the Degree

MASTER OF PUBLIC HEALTH

Concentration: Epidemiology

ATLANTA, GEORGIA

30303

APPROVAL PAGE

SUB-EPIDEMIC GENERALIZED LOGISTIC-GROWTH MODEL PERFORMANCE FOR INFLUENZA SEASON IN THE UNITED STATES, OCTOBER 2015–APRIL 2019

by

Hannah E. Fast

Approved:

Dr. Gerardo Chowell

Committee Chair

Desiree Mustaquim

Committee Member

December 15, 2020

Date

Author's Statement Page

In presenting this thesis as a partial fulfillment of the requirements for an advanced degree from Georgia State University, I agree that the Library of the University shall make it available for inspection and circulation in accordance with its regulations governing materials of this type. I agree that permission to quote from, to copy from, or to publish this thesis may be granted by the author or, in his/her absence, by the professor under whose direction it was written, or in his/her absence, by the Associate Dean, School of Public Health. Such quoting, copying, or publishing must be solely for scholarly purposes and will not involve potential financial gain. It is understood that any copying from or publication of this dissertation which involves potential financial gain will not be allowed without written permission of the author.

Hannah E. Fast
Signature of the Author

TABLE OF CONTENTS

LIST OF FIGURES

LIST OF TABLES

CHAPTER I – INTRODUCTION

1.1 Description of the Public Health Problem

The emergence of an infectious disease outbreak poses serious risks for the health and well-being of susceptible populations. An outbreak begins as a cluster of cases, epidemiologically linked by time and place, that exceeds the endemic prevalence for the area (CDC, 2011). Without public health intervention, an outbreak often shows exponential growth and can quickly become an epidemic, a term indicating wider geographic spread, and eventually evolve into a pandemic after achieving infections across multiple countries. Extensive, epidemic spread is likely to have severe health, economic, and social consequences if transmission cannot be brought under control. For this reason, epidemics are best dealt with preemptively and the strength of the response benefits from early identification and institution of swift public health interventions. Interventions encompass a wide range of policies and recommendations, such as mandatory quarantines, school closures, outbreak vaccination clinics, travel restrictions, product recalls, and limitations on the movement and sale of livestock.

To design effective interventions, public health researchers and authorities must recognize that the response to an infectious disease does not occur in a vacuum; it occurs in a highly complex social, political, and economic environment. Thus, designing an intervention in theory can be much different than in practice, as each occurrence of an outbreak brings its own idiosyncratic set of challenges. In 1990, sociologist Philip Strong observed the extraordinary ways in which epidemics, referring to both the spread of disease and the strategies put in place to control spread, disrupt public order and create the "medical version of a Hobbesian nightmare – the war of all against all." With such serious consequences, it is essential that all public health

recommendations are grounded in scientific knowledge and that the processes for developing that knowledge are widely validated and understood.

Amidst the challenges posed by an epidemic, the public health goal remains to derive accurate, meaningful, and expert information from the constantly evolving stream of epidemiologic data that is generated. The ability to rapidly disseminate accurate epidemiologic research and analysis in a quickly evolving infectious disease outbreak or epidemic situation is crucial to intervention development. This information will be used to make difficult decisions regarding how to balance the costs and benefits of preventative measures, how to gain funding and access to resources, and how to communicate to the public.

There have been extensive efforts in the field of epidemiology over the past few centuries to specifically define what epidemiologic information is needed during an epidemic response. Public health professionals are trained to use descriptive epidemiology to identify details regarding the elements of person, place, and time (CDC, 2011). Brockmann and Helbing in 2013 developed these concepts further and described four key questions public health authorities must ask in the event of an epidemic with potential for global spread:

"1) Where did the [novel] pathogen emerge?

2) Where are new cases to be expected?

3) When is an epidemic going to arrive at distant locations?

4) How many cases are to be expected?"

Three of the four questions involve some degree of prediction to determine where, when, and to what extent the epidemic will spread. These predictions are likely to be informed by statistical models, which are used to explore the relationship between an independent and a dependent variable, predict outcomes, and determine the likelihood and error around that

outcome (Casals, Giraben-Farrés & Carrasco, 2014). Models are useful tools because they simplify the complexity of transmission dynamics, allowing application to disparate geographic regions, populations, and circumstances (Vynnycky & White, 2010).

In addition to defining relevant research questions, public health authorities also need to be familiar with what data sources are available, as well as the time and resources required to analyze the data to create meaningful, accurate findings. Questions to ask include: are existing data sources sufficient or is the development of new data collection methods required? How reliable are existing data sources? How much time would it take to develop new methods of data collection, such as a survey or case report form? Useful epidemiologic analysis depends on the identification of accurate data sources, as well as existing capacity for data access and transmission among public health and healthcare partners. It also depends on a skilled workforce for appropriate scientific analysis and the ability to successfully translate scientific findings into information that can be consumed by a variety of audiences.

In recent years, public health has increasingly sought to develop advanced technological methods and utilize big data for epidemiologic purposes. Vast technological advances in other sectors of society have allowed for increased collection of health, demographic, and social networking information, resulting in a proliferation of novel data sources for incorporation into epidemiologic investigation and research. Forays into the use of big data to answer these key questions in the event of an outbreak offer exciting and promising results. Some of the developments in this field include researchers looking to implement complex and unsupervised machine learning processes (Waldner, Osgood & Seitzinger, 2017). However, increased access to data comes with the important caveat that more data does not always correlate to better results. There are several important limitations that may not make these advanced methods suitable for

all agencies and all public health responses. Novel data sources might not be able to be reconciled with official or validated sources. National infectious disease surveillance systems and infrastructure, such as the National Notifiable Diseases Surveillance System, are limited in scope by interoperability challenges and the cost of updating data standards and collection (Garcia et al., 2018). Furthermore, analysis of big data requires expert data management skills and the ability to translate existing data fields into the form that is needed to answer scientific questions. Appropriate use of big data can be severely limited by a shortage of computational resources, lack of skilled staff, and challenges in validating and communicating the results. While fully acknowledging the value of these technological advances, there is still a justified need to examine how to efficiently and accurately obtain epidemiologic information from relatively simple, validated, and consistent data sources.

The United States recently saw the importance of early-time infectious disease models during the development of the novel COVID-19 pandemic in February and March 2020. In March, U.S. governors, including Jay Inslee of Washington[1], Gavin Newsom of California[2], and Andrew Cuomo of New York[3], chose to make the difficult decision to implement mandatory school and business closures and stay-at-home orders, with much of the U.S. following in their footsteps shortly after. These high-risk decisions, for which the extent of the impact has yet to be determined, were justified by caseload predictions informed by models. The global development of COVID-19 reaffirms the importance of developing and validating infectious disease models

[1] Example of March 2020 media coverage of Washington COVID-19 models: https://www.seattletimes.com/seattle-news/how-about-without-intervention-400-could-die-from-coronavirus-in-western-washington-by-april-7-study-suggests/
[2] California example: https://www.nytimes.com/2020/03/19/us/California-stay-at-home-order-virus.html
[3] New York example: https://www.nytimes.com/2020/03/31/world/coronavirus-live-news-updates.html

prior to the emergence of major public health emergencies. This ensures officials will have the information necessary to prevent morbidity, mortality, and other harms related to well-being.

1.2 Research Aim

This study aims to evaluate a sub-epidemic version of the generalized logistic-growth model (GLM) developed by Chowell and Tariq (2019). The model will be fit to a delineated period of epidemic growth within four influenza seasons, using U.S. influenza-like illness (ILI) weekly incidence as a proxy. The study will compare the model performance results between the GLM with 1 sub-epidemic curve to the modified GLM with 2 and 3 sub-epidemic curves. The intent is to validate how incorporation of sub-epidemics into the model affects the utility of the GLM for use on government case reporting data. The hypothesis is that the sub-epidemic model will perform better than the single curve GLM. Gathering support for this model will help strengthen the use of sub-epidemic methodology as a relatively quick and scalable approach to improve understanding of epidemic growth dynamics and inform public health response efforts.

CHAPTER II – LITERATURE REVIEW

2.1 Risk Assessment in an Epidemic

A sudden, unexpected rise in cases of an infectious disease is a cause for concern due to the uncertainty of risk involved and the potential for harmful outcomes. The World Health Organization (WHO) and other prominent scientific institutions have used the precautionary principle framework to establish the necessity of public health action in an emergency despite the presence of scientific uncertainty (Martuzzi and Tickner, 2004). In summary, the principle posits, "in cases of serious or irreversible threats to the health of humans or ecosystems, acknowledged scientific uncertainty should not be used as a reason to postpone preventative measures" (Martuzzi and Tickner, 2004). The uncertain circumstances that surround the rapid development of an infectious disease outbreak make the precautionary principle applicable. For example, when the 2003 SARS epidemic began, little was known about the disease (Bensimon & Upshar, 2007). In Singapore, introduction of 1 index case into a hospital rapidly evolved into a healthcare outbreak of 109 cases, despite infection control measures, and then spread into the community (Goh, Cutter, & Heng et al., 2006). The demonstrated risk, despite scientific uncertainty, justified implementation of strict control measures such as the closure of a 24-hour market and mandatory quarantine of thousands who may have been exposed (Goh, Cutter, & Heng et al., 2006). Subsequent analysis of the SARS outbreak in Singapore shows that the rapid control measures were effective in slowing the spread. Lipsitch et al. (2003) found an initial effective reproductive number of R=7 in the first week of the Singapore outbreak, later declining to R=1.6 in the second week and R <1 in following weeks. Precautionary action to introduce control measures in a high-risk situation ultimately reduced harm to the community and was able to control and stop spread of the disease.

As the precautionary principle is defined broadly and theoretically, there is much discussion within the scientific and legal community about how to apply the principle objectively. Critics of the principle argue that aggressive use of precaution can be harmful, (Wilson et al., 2019) while others have made the case that historically, existing assumptions about causality, which precautionary action might draw upon, have had to be overturned in order to stop disease transmission and advance scientific understanding (Goldstein, 2012). From a legal perspective, Kegge (2020) argues a standard of proof must be met to use the precautionary principle as justification. That standard is based on a risk assessment that shows a significant level of risk. In other words, evoking the precautionary principle requires a threshold of severity. In an outbreak, this implies that the consequences of uncontrolled disease spread to the public's health must outweigh any potential costs or damage caused by control measures (Fischer & Ghelardi, 2016). Overall, outbreak response is highly dependent on accurate and validated methods of estimating risk.

Risk assessments during the early growth period of an epidemic are often informed by mathematical models (Chowell et al., 2016b). Statistical models that use principles of exponential growth are able to define the relationship between cases of disease and time, providing insight into transmission dynamics. This information makes it possible to gauge the severity of the health threat by estimating epidemic size, anticipated growth rate, and the likelihood of clinical outcomes such as hospitalization, disability, and death. During the early stage of an epidemic, when data on case-patient outcome is likely to be incomplete, models may be able to provide more accurate information than crude calculations. For example, during onset of COVID-19, Verity et al. (2020) estimated case fatality rates using a parametric model because

the crude case fatality rates calculated during past respiratory disease epidemics (e.g., SARS and H1N1 influenza) were later found to be underestimated.

A wide range of different model structures are used within the field of infectious disease modeling. Thus, after defining the research question and appropriate data sources, analysis design must take into account how to select an appropriate model structure for the investigation. Vynnycky & White (2010) describe the process of choosing a model structure as dependent on the natural course of the infection and the time period being investigated. For example, a model structure will need to take into consideration the length of the incubation period and whether infected individuals will return to the susceptible population. If this information is not available, as is the case with a novel pathogen, or data is incomplete, parsimonious models are able to account for these limitations by incorporating built-in assumptions into the model.

The exponential growth model is a phenomenological model, which means it is a mathematical model that can describe the relationship between an independent and dependent variable (Chowell et al., 2016a). A phenomenological model is able to derive all of the necessary information from case count data because it makes assumptions about the transmission based on mathematical principles of exponential growth, rather than parameters that need to be defined based on an understanding of the natural history of the infection. This makes the model a promising candidate for use in situations where data is limited, such as the case of a novel epidemic where existing knowledge on the disease is limited. The exponential growth model is able to provide meaningful information during the initial phase of outbreak when case counts grow exponentially within the population and outcomes such as recovery and death are still limited (Bertozzi et al., 2020). Bertozzi et al. (2020) identified exponential growth as a one of three parsimonious models that was effective to use with COVID-19 early-time local and

national government case data. Their selection of the model was based on the criteria that the model be relatively simple, require few parameters, and have the ability to be scaled to accommodate varying region sizes.

Epidemics often show exponential behavior during the growth period, such as the 2014 Ebola epidemic (Hunt, 2014) and the 2009 H1N1 pandemic (de Picoli Junior et al., 2011). It is also common to see sub-exponential behavior, depending on the circumstances in which the epidemic is occurring. For example, sub-exponential behavior was observed during the emergence of COVID-19 in mainland China (Maier & Brockmann, 2020) and Ebola in Uganda (Viboud, Simonsen & Chowell, 2016). The generalized logistic-growth model distinguishes between exponential and sub-exponential growth by the inclusion of a growth scaling factor into the model (Viboud, Simonsen & Chowell, 2016). This allows the model to be scaled to a many different diseases and situations.

2.2 Sub-epidemic Model Development

Chowell and Tariq (2019) introduced a novel sub-epidemic modeling framework that aggregates multiple sub-epidemic curves to better fit overall incidence data. In the initial investigation, the sub-epidemic model was found to perform better than simple logistic-growth models when applied to historical outbreaks of SARS, Ebola, and Plague. The sub-epidemic model is fit to epidemic curve data. The epidemic curve, a histogram which shows incidence of cases over time, is one of the simplest tools used frequently by epidemiologists (CDC, 2011). The epidemic curve has remained a foundational tool for summarizing the distribution of cases because it is multi-functional and mathematical analysis of the epidemic curve is able to provide information about modality, generation time, and growth rate. In reality, the growth of an

epidemic is complex, with transmission occurring in various settings and among different populations with different beliefs and types of social interactions. The sub-epidemic model identifies mathematical variation within an aggregate epidemic curve and highlights ways the distribution might be broken down to show differences in transmission dynamics between sub-populations. This information could be used to identify different transmission settings, target interventions, and generate hypotheses. While visual analysis of the epidemic curve is able to provide some answers to the key questions during an epidemic, mathematical analysis informed by a model will be able to provide more comprehensive epidemiologic information.

The sub-epidemic model is a modified version of the generalized logistic-growth model (GLM) that creates estimates for a specified number (n) of sub-epidemics within one overall epidemic curve (Chowell & Tariq, 2019). Model fit is determined by aggregating the sub-epidemics and comparing the fit of the aggregate curve to the actual data. Figure 1 contains an example of the differences between these two approaches, with 1 GLM curve on the left compared to an aggregated curve from 2 sub-epidemics on the right. It is important to note in Figure 1 that both models were generated using the same source data. The model estimates three parameters for each sub-epidemic: r, the growth rate, p, a growth scaling factor, and K, the total epidemic size. Thus, the total number of parameters estimated for the model will be $3n$, or 3 times the number of sub-epidemics. Increased parameters come at a cost to the model's utility. As the model derives all of its information from the available data, parameter estimation becomes less reliable as more parameters are required to be estimated. The multiplication of parameters as the number of sub-epidemics increases can lead to parameter identifiability challenges and increase model uncertainty (Roosa & Chowell, 2019).

When the number of sub-epidemics is 1 (n=1), the model represents the GLM, with equation $\frac{dC(t)}{dt} = r \times C(t)^p \times (1 - \frac{C(t)}{K})$ and *C(t)* representing the incidence over time. As shown on the right in Figure 1, only one curve is generated to fit the data. As the number of sub-epidemics increases, the equation incorporates an index, *i*: $\frac{dC_i(t)}{dt} = r_{i-1} \times C_i(t)^p \times (1 - \frac{C_i(t)}{K_i})$. In the sub-epidemic version, multiple curves using the GLM equation are used to fit the data.

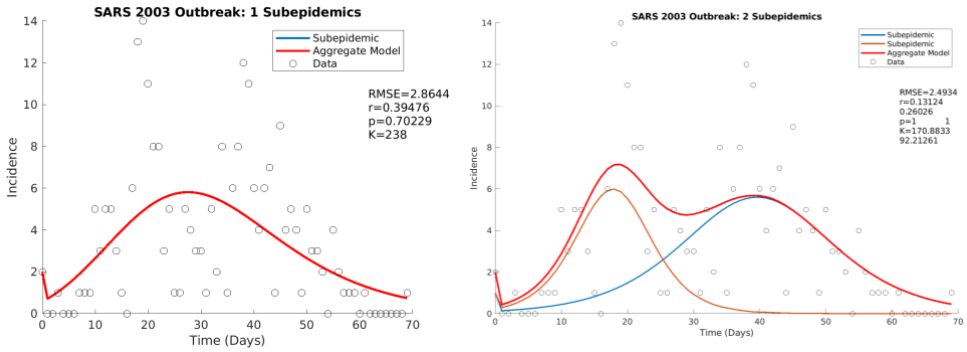

Figure 1 Example of sub-epidemic curve aggregation using SARS outbreak data, for n=1 and n=2.

2.3 Application to Seasonal Influenza

Influenza is a viral respiratory disease caused by the family of influenza viruses, including influenza A and influenza B viruses. Transmission dynamics for influenza are complex, partially due to frequent mutations and circulation of multiple strains, and partially due to the effect of environmental and behavioral changes on influenza transmission (Lofgren et al., 2007). There is an observed seasonality to influenza spread in the United States, with increased transmission beginning in the fall and winter months of each year. The seasonality occurs for several reasons, including the effect of humidity and temperature on spread (Lowen et al., 2007) and increased human susceptibility and the increase in behavior (e.g., crowding) that is conductive to spread (Lofgren et al., 2007). Thus, although influenza is being transmitted year-

round, periods of epidemic growth occur due to both the effect of seasonality and potential introduction of new strains into susceptible populations.

For influenza, the average generation time is 3 days (Nasserie et al., 2017). This means that fluctuations in growth rate can cause epidemics of high magnitude quickly. It is often identified as the pathogen of interest in planning for novel pandemics because the disease is "more likely to occur than other pathogen types and which is also relatively likely to result in a large epidemic" (Biggerstaff et al., 2019). With national surveillance data delayed by 1 to 2 weeks, staying aware of influenza transmission dynamics to provide nowcasts and forecasts is important for situational awareness (Leuba et al., 2020). Severity assessments of influenza inform resource distributions of vaccination, hospitalization bed availability, antivirals, and assist with communication to the public (Barr & Cheng, 2018). The sub-epidemic GLM is one approach to assess influenza dynamics in real time and inform public health response.

CHAPTER III – METHODS AND PROCEDURES

3.1 Influenza-like Illness (ILI) Surveillance Data

The national surveillance system for influenza activity in the U.S. includes eight components and monitors five types of data sources: virologic testing, outpatient visits, geographic spread of disease, hospitalizations, and mortality reporting (National Center for Immunization and Respiratory Diseases [NCIRD], 2020a). One of these components is the U.S. Outpatient Influenza-like Illness Surveillance Network (ILINet), which is comprised of nearly 3,000 outpatient healthcare providers that voluntarily report to CDC weekly. ILINet surveillance data includes the total number of outpatient visits to the provider per week and of these, the number of patients with ILI. ILI is defined as a fever greater than 100º F and cough and/or sore throat, without another known cause (NCIRD, 2020a). It is important to note that ILINet counts are not laboratory-confirmed and should not be interpreted as influenza incidence, as ILI is non-specific and could potentially have another cause. In addition, only a subset of healthcare providers participates in the surveillance system and many individuals do not seek out healthcare or receive laboratory testing for influenza when ill. While measures of ILI do not capture the magnitude of influenza transmission, fluctuations in ILI activity over time can be used as a proxy to study overall patterns and trends in the influenza season (World Health Organization [WHO], 2015). Thus, because the logistic-growth model captures growth dynamics over time, the change in ILI counts from week to week can offer insight into seasonal dynamics for influenza.

ILINet summary-level data are published on two FluView Interactive dashboards[4,5] and made available for public use. For this investigation, national ILI counts by week were obtained

[4] National, Regional, and State Level Outpatient Illness and Viral Surveillance: https://gis.cdc.gov/grasp/fluview/fluportaldashboard.html

[5] Age Group Distribution of Influenza Positive Tests Reported by Public Health Laboratories: https://gis.cdc.gov/grasp/fluview/flu_by_age_virus.html

from FluView Interactive for four influenza seasons: 2015–2016, 2016–2017, 2017–2018, and 2018–2019. Data on virus characterization, age group, and geographic region were also obtained for supplemental analysis.

Since ILI activity occurs year-round, the fall and winter influenza season for each year was delineated and analyzed as an epidemic period. The epidemic period was defined beginning in early October at Morbidity and Mortality Weekly Report (MMWR) Week 40, which is the start of the influenza reporting period for each season, through late April, MMWR Week 17, of the next year (NCIRD, 2020a). Each season contained a total of 30 data points. The specific start and end dates for each season are listed in Table 1. A baseline adjustment was made so that the ILI incidence for all 30 weeks within the season was decreased by 1 less than the epidemic week 0 incidence. After the adjustment, each epidemic period started at a count of 1 (Figure 3). This was done to counter the inflation of growth dynamics for the first data point, which occurred when the epidemic period was removed from seasonal context and no longer able to be analyzed in relation to the preceding week.

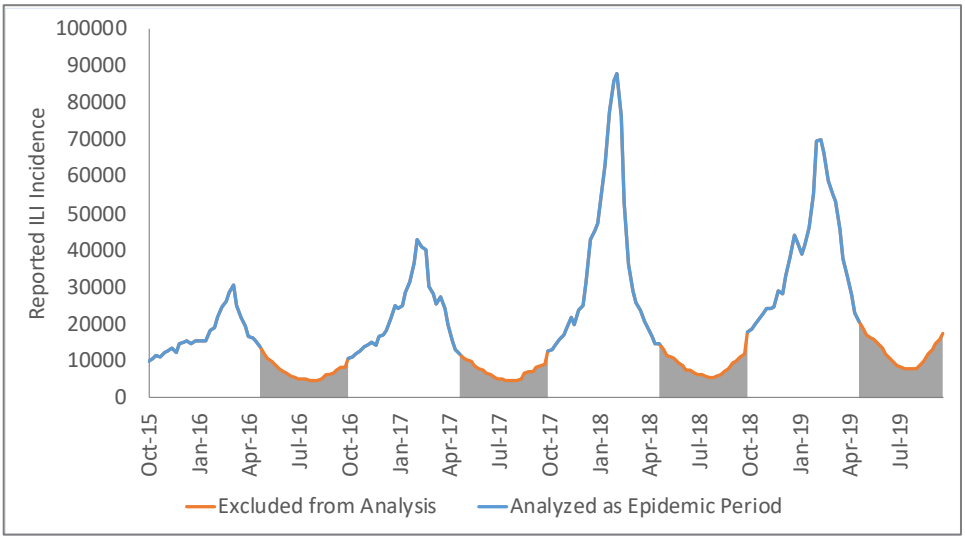

Figure 2 Influenza seasons were delineated by week of report and analyzed as an epidemic period. Each season started in early October (MMWR Week 40) and ended in late April (MMWR Week 17) of the next year.

Table 1 Date of start, peak, and end of the delineated seasons. The date corresponds to the Saturday at the end of the week of report (MMWR Week).

Season	Week of Season Start / MMWR Week (Date)	Week of Season Peak / MMWR Week (Date)	Week of Season End / MMWR Week (Date)	# Data Points
2015–2016	0 / 40 (10-10-15)	22 / 10 (3-12-16)	29 / 17 (4-30-16)	30
2016–2017	0 / 40 (10-8-16)	18 / 6 (2-11-17)	29 / 17 (4-29-17)	30
2017–2018	0 / 40 (10-7-17)	18 / 6 (2-10-18)	29 / 17 (4-28-18)	30
2018–2019	0 / 40 (10-6-18)	19 / 7 (2-16-19)	29 / 17 (4-27-19)	30

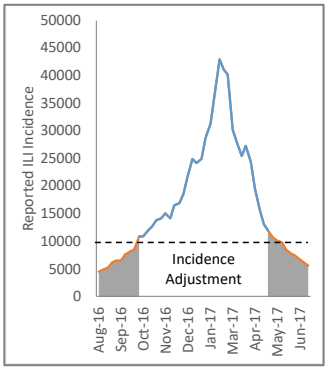

Figure 3 The reported ILI incidence was adjusted so that each season started at a value of 1.

3.2 Fitting the Model

Analysis was conducted using MATLAB, with code development supported by Dr. Gerardo Chowell and Kimberlyn Roosa at Georgia State University School of Public Health. The sub-epidemic generalized-logistic growth equation, $\frac{dC_i(t)}{dt} = r_{i-1} \times C_i(t)^p \times (1 - \frac{C_i(t)}{K_i})$, was created into a function. A simple two column matrix with time in one column and case counts in another was created for each epidemic period, and prior to analysis, the measure of time was converted from weeks to days. Parameter values were estimated for *r*, the growth rate, *p*, the growth scaling factor, and *K*, the total epidemic size, for *n* sub-epidemics. The number of sub-epidemics was specified as 1, 2, and 3 sequentially for each dataset, which resulted in estimation of 3, 6, and 9 parameters, respectively. Parameter estimates were obtained through nonlinear least squares curve-fitting of the epidemic period using the MATLAB *lsqcurvefit* function. This function identifies the set of parameters that produce a model with the least summed differences

between the estimated data point and the actual source data at each point in time (Roosa & Chowell, 2019). Starting parameter estimates for the least squares curve-fitting process were randomly generated from a continuous uniform distribution using the *unifrnd* function in MATLAB. Since the solver is sensitive to the starting values, the random generation of these values meant model outcomes often differed across runs. To account for this, each model scenario was generated a minimum of 10 times and the best fit for that scenario was chosen using a comparison of residuals, performance metrics, and parameter identifiability metrics, as described in a following section. Upper and lower bounds for the parameters were defined as follows: $0 < r < 10$; $0 < p < 1$; $1 < K <$ cumulative count for the epidemic period. C(t) was defined as the starting incidence divided by the number of sub-epidemics (n).

After the best fit parameter estimates were identified, an ordinary differential equation solver (*ode45* function in MATLAB) used these estimates to calculate cumulative incidence curves for each sub-epidemic. Cumulative incidence was transformed into weekly incidence and plotted. Finally, weekly incidence for all sub-epidemics was summed to produce the aggregate model.

Parametric bootstrapping was conducted to provide additional information on model fit and parameter identifiability metrics. During the bootstrapping process, two hundred simulated datasets were generated from the aggregate incidence curve using a Poisson error structure. Then, the model fit process was repeated for each simulated dataset, which resulted in 200 estimates for each parameter value and 200 incidence curves. These curves were used to calculate a 95% CI around the model and the best fit parameter value.

3.3 Model Comparison and Performance Metrics

Four performance metrics were used to assess model fit: root-mean-square error (RMSE), mean absolute error (MAE), mean interval score (MIS), and 95% confidence interval (CI) percent coverage (Chowell & Tariq, 2019). All four metrics were used together to provide a comprehensive assessment of model performance. In addition, qualitative and visual analysis of fit, residual variance, and parameter confidence interval widths also informed model selection and interpretation.

The RMSE and MAE are statistics that measure the average magnitude of distance between the model and the underlying data point (Willmott & Matsuura, 2005). The RMSE equation averages the squared residuals and then takes the square root. This is represented in the following equation, $RMSE = \left[\sum_{i=0}^{n} \left(z_{f_i} - z_{o_i}\right)^2 / n\right]^{1/2}\right]$ (Barnston, 1992). The MAE takes the absolute value of the residuals, $MAE = \left[\sum_{i=0}^{n} \left|z_{f_i} - z_{o_i}\right|\right]$ (Willmott & Matsuura, 2005). Since both the RMSE and MAE represent the magnitude of the residuals, lower values for these metrics indicate better model performance because a better fit to the data will minimize the distance between the model and data points. Qualitative analysis of the distribution of residuals also informed model selection. Model fits with residuals showing constant variance and random distribution were preferred over model fits showing residuals with nonconstant variance, even if RMSE and MAE were similar in magnitude. These three methods of evaluation were applied to the best fit models.

The remaining two metrics, MIS and 95% CI percent coverage, were obtained after the bootstrapping process. The MIS calculates the width of the 95% confidence interval generated from the 200 model curves that were fit to the simulated datasets. The metric scores whether or not data points fall into that interval and how close they fall to the bounds. The MIS follows the

equation, $MIS = \frac{1}{h}\sum_{i=0}^{h}(U_{t_i} - L_{t_i}) + \frac{2}{0.05}(L_{t_i} - y_{t_i})I\{y_{t_i} < L_{t_i}\} + \frac{2}{0.05}(y_{t_i} - U_{t_i})U\{y_{t_i} < U_{t_i}\}$ (Chowell & Tariq, 2019). If the data point falls outside the lower or upper bounds of the interval, it is assigned 1 point. In addition, the MIS incorporates a calculation of the difference between the upper and lower bounds, meaning that narrow intervals will have a lower score while wider intervals will have a higher score. Overall, a lower MIS indicates better performance. Lower scores are obtained from a narrower 95% CI with less variation and may also be indicative of the 95% confidence interval's ability to represent the underlying data points. Similarly, the 95% CI percent coverage captures the percent of data that falls into the bounds of the 95% CI. A model with high percent coverage indicates a good fit while decreasing percent coverage would be interpreted as weaker model performance. Comparison of the width of the 95% CI around the parameter estimates provided information about parameter identifiability, with a wider 95% CI indicating increased uncertainty around the value of the estimate (Roosa & Chowell, 2019).

CHAPTER IV – RESULTS

4.1 Description of Epidemic Curves

The growth curve of reported ILI incidence was skewed left for all four seasons, with epidemic peak occurring after the midway point, at epidemic week 22, 18, 18, and 19 for the 2015 to 2018 seasons, respectively. The 2018–2019 season had the highest cumulative incidence of ILI, closely followed by the 2017–2018 season, which also had the steepest curve and highest peak. The 2015–2016 season had both the latest peak and the lowest peak.

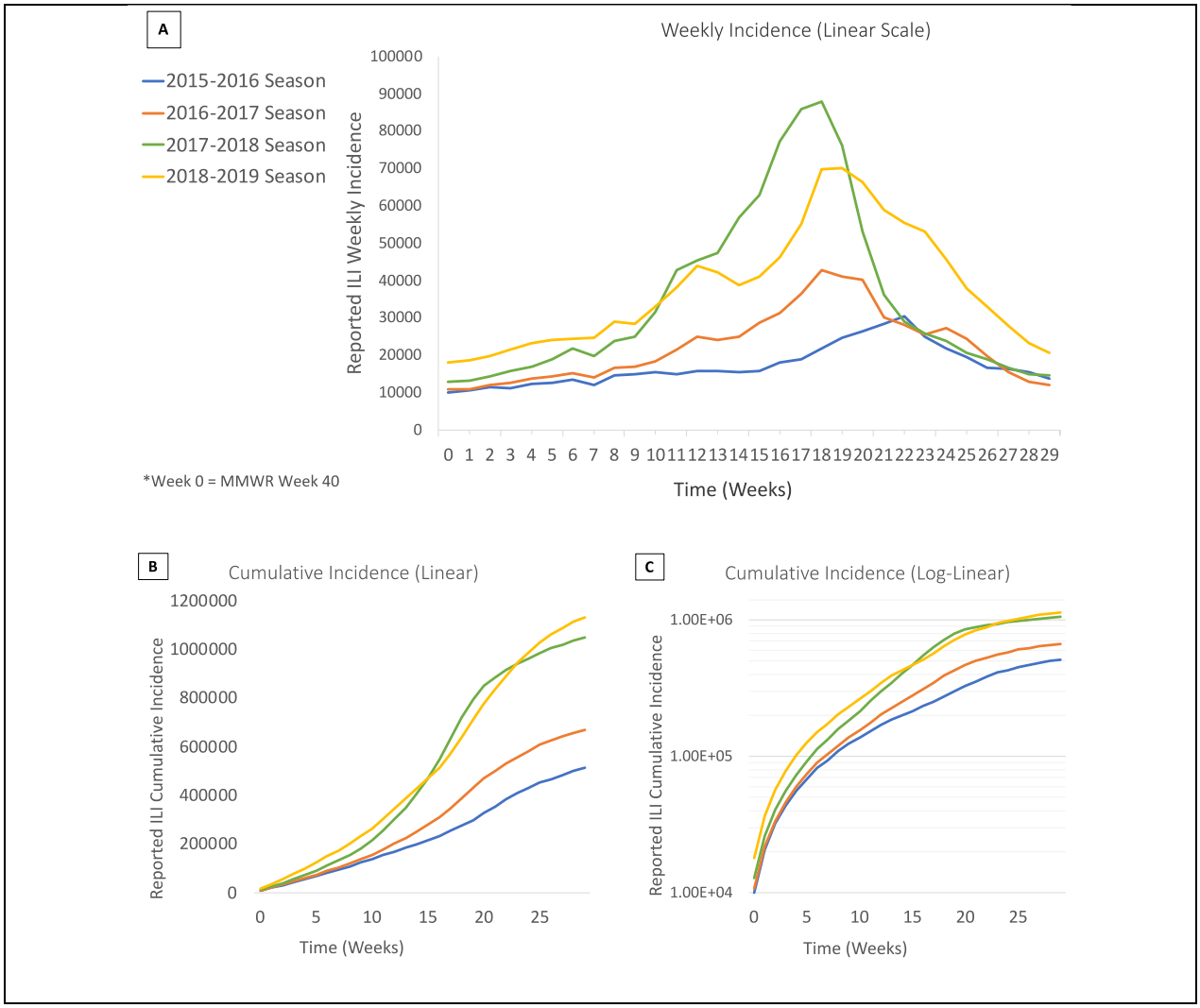

Figure 4 Comparison of ILI trends across years. This figure represents reported incidence, not adjusted. A) Weekly incidence on a linear scale. B) Cumulative incidence on a linear scale. C) Cumulative incidence on a log-linear scale.

4.2 Parameter Estimates

Across the four years that were analyzed, best fit estimates for *r*, the growth rate, ranged from 0.0695 to 6.33, with a median of 0.2485. Best fit estimates for *p*, the growth scaling factor, ranged from 0.466 to 1.00, with a median of 0.8845. Lastly, best fit estimates for *K*, total epidemic size, ranged from 5,353 to 627,515, with a median of 166,167. Best fit estimates from each model are shown in Figure 5 and Table 2.

With the sub-epidemic model, parameter estimates are expected to vary within one season as sub-epidemics can take many different shapes within an aggregate curve. However, there are observable patterns across parameter estimates related to the shape of the aggregate curve. For example, the 2015–2016 season had both the highest estimates for *r* and the lowest estimates for *p* of the four years. Although the overall shape of this curve is the most gradual of all the seasons, it had the latest peak and therefore the longest left tail. The sub-epidemic curve generated to fit this tail had a high *r* value (6.33 for 1 curve when n=2; 6.23 for 1 curve when n=3) but when paired with a low *p* (0.473 for 1 curve when n=2; 0.466 for 1 curve when n=3), this created a wide and gradual curve. This relationship between *r* and *p* was also seen in the 3 sub-epidemic model of the 2018–2019 season, where a relatively high *r* value (2.877 for 1 curve when n=3) was paired with a relatively low *p* value (0.633 for 1 curve when n=3) to create a small and gradual curve to fit the skewed left tail of that season.

The 2017–2018 season had the highest peak and the steepest incline. This resulted in the largest estimate for *K*, total epidemic size, when n=1 because the one sub-epidemic curve generated also had a high peak. Individual estimates for *K* typically decreased as the number of sub-epidemics increased, as the aggregate incidence curve would then have multiple sub-epidemics contributing to its height and shape.

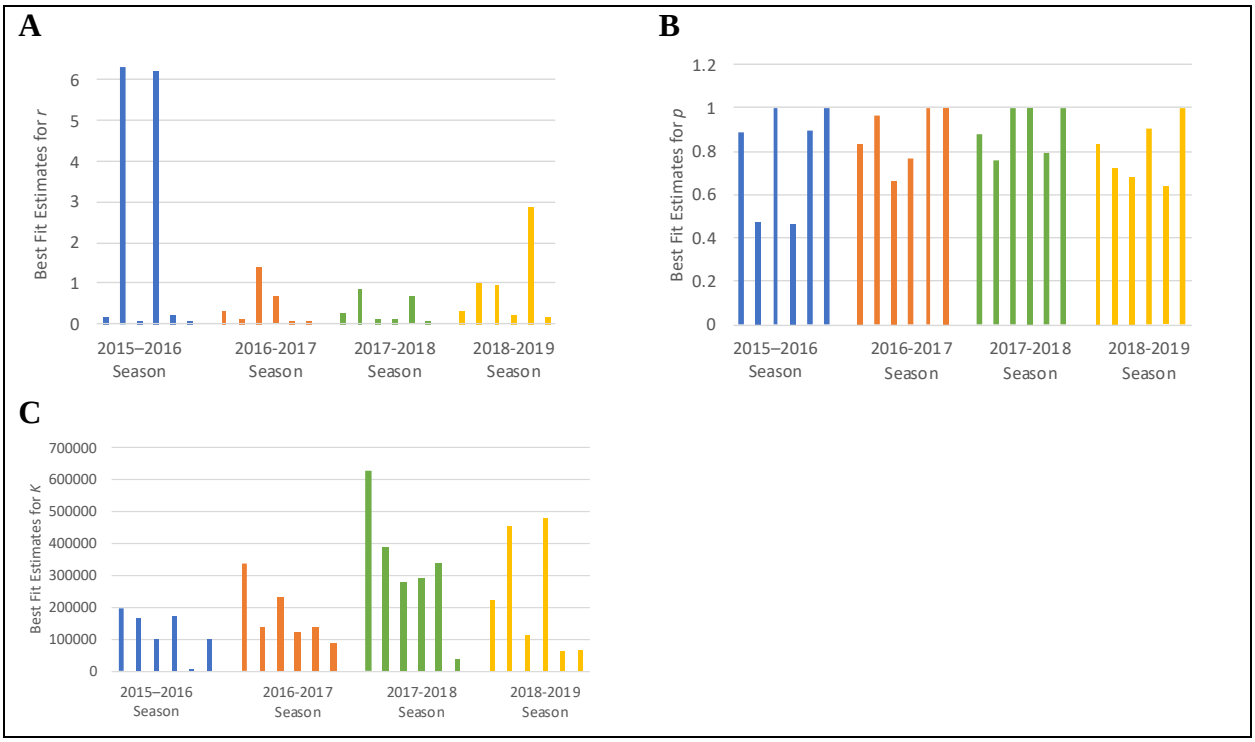

Figure 5 Distribution of sub-epidemic parameter estimates obtained from the best fit model. A) Estimates for *r*, the growth rate. B) Estimates for *p*, the growth scaling factor. C) Estimates for *K*, total epidemic size.

Table 2 Values for sub-epidemic parameter estimates obtained from the best fit model.

Season	Model Type	Growth Rate (*r*)	Growth Scaling Factor (*p*)	Total Epidemic Size (K)
2015–2016	GLM 1 Sub-Epidemic	r: 0.180	p: 0.887	K: 195,728
	GLM 2 Sub-Epidemics	r_1: 6.33	p_1: 0.473	K_1: 163,407
		r_2: 0.0839	p_2: 1.00	K_2: 98,353
	GLM 3 Sub-Epidemics	r_1: 6.23	p_1: 0.466	K_1: 168,926
		r_2: 0.218	p_2: 0.894	K_2: 5,353
		r_3: 0.0885	p_3: 0.996	K_3: 99,417
2016–2017	GLM 1 Sub-Epidemic	r: 0.330	p: 0.837	K: 336,989
	GLM 2 Sub-Epidemics	r_1: 0.116	p_1: 0.967	K_1: 133,615
		r_2: 1.40	p_2: 0.667	K_2: 232,218
	GLM 3 Sub-Epidemics	r_1: 0.675	p_1: 0.767	K_1: 120,095
		r_2: 0.104	p_2: 0.997	K_2: 137,775
		r_3: 0.0775	p_3: 0.998	K_3: 84,230
2017–2018	GLM 1 Sub-Epidemic	r: 0.279	p: 0.882	K: 627,515
	GLM 2 Sub-Epidemics	r_1: 0.881	p_1: 0.755	K_1: 386,564
		r_2: 0.111	p_2: 1.00	K_2: 275,307
	GLM 3 Sub-Epidemics	r_1: 0.113	p_1: 1.00	K_1: 289,733
		r_2: 0.676	p_2: 0.788	K_2: 334,404
		r_3: 0.0695	p_3: 1.00	K_3: 34,211
2018–2019	GLM 1 Sub-Epidemic	r: 0.331	p: 0.831	K: 223,450
	GLM 2 Sub-Epidemics	r_1: 1.01	p_1: 0.720	K_1: 449,210
		r_2: 0.951	p_2: 0.680	K_2: 108,699
	GLM 3 Sub-Epidemics	r_1: 0.204	p_1: 0.900	K_1: 478,771
		r_2: 2.877	p_2: 0.633	K_2: 61,192
		r_3: 0.154	p_3: 1.00	K_3: 63,499

4.3 Model Performance Metrics

The performance metric results represent model outcomes from both the least squares curve-fitting process and the bootstrapping process. As the number of sub-epidemics incorporated into the model increased, the magnitude of error as measured through RMSE and MAE decreased. MIS also showed a consistent decrease, indicating that the 95% CI around the best fit model became narrower as the number of sub-epidemics increased. Overall, the model 95% CI did not capture a high percentage of the underlying data, with a maximum of 17%. For two seasons, 2015–2016 and 2016–2017, percent coverage slightly increased as number of sub-epidemics increased. For the other two seasons, 2017–2018 and 2018–2019, percent coverage stayed consistent for all values of *n*. The results for fit, residual variance, and width of 95% CI around parameter estimates are included in season-specific figures.

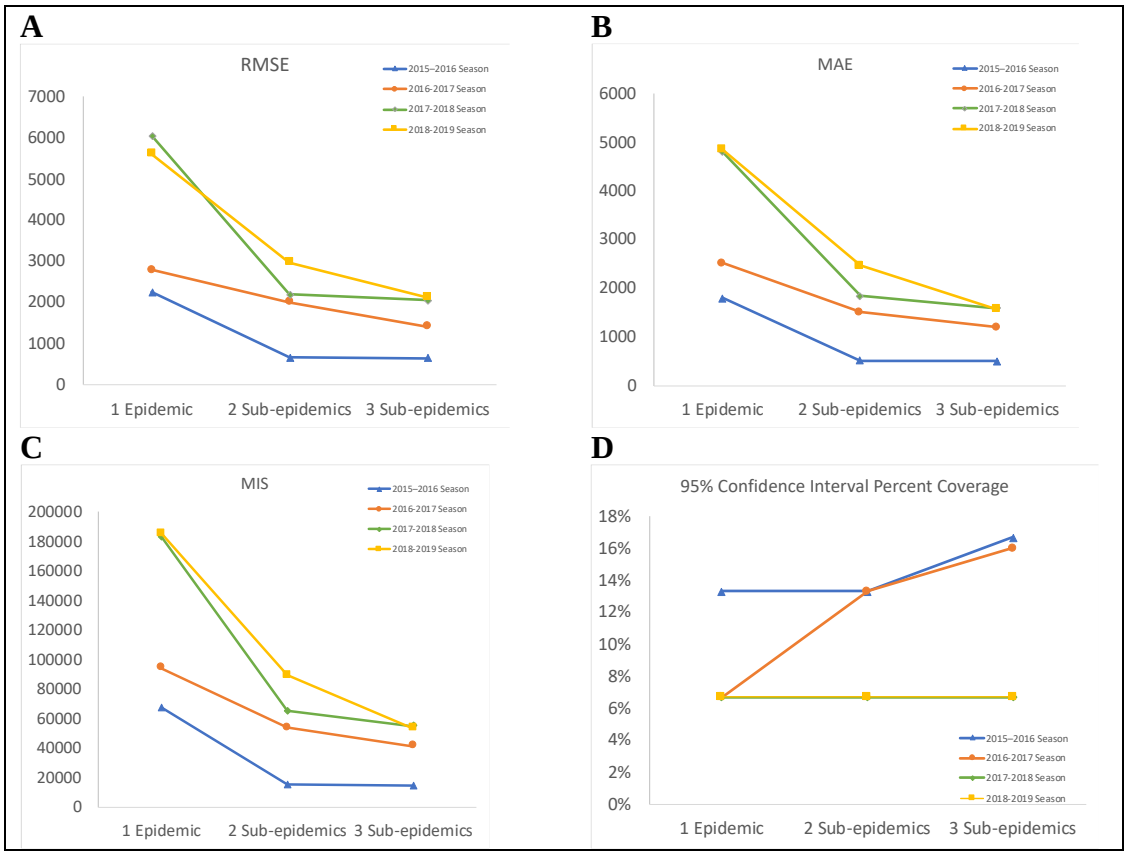

Figure 6 Model performance metrics for four seasons with number of sub-epidemics increasing from *n*=1 to *n*=3. A) RMSE results. B) MAE results. C) MIS results. D) 95% CI percent coverage results.

Table 3 Model performance metrics for the four seasons.

Season	Model Type	RMSE	MAE	MIS	95% CI Coverage
2015–2016	GLM 1 Sub-Epidemic	2246.8	1794.6	67416	13.3%
	GLM 2 Sub-Epidemics	667.9	519.1	15499	13.3%
	GLM 3 Sub-Epidemics	654.1	500.2	14782	16.7%
2016–2017	GLM 1 Sub-Epidemic	2793.0	2516.3	94311	6.7%
	GLM 2 Sub-Epidemics	2005.4	1511.5	54052	13.3%
	GLM 3 Sub-Epidemics	1417.4	1194.6	41337	16.0%
2017–2018	GLM 1 Sub-Epidemic	6043.4	4789.2	183221	6.7%
	GLM 2 Sub-Epidemics	2193.6	1841.6	65133	6.7%
	GLM 3 Sub-Epidemics	2052.3	1586.2	55241	6.7%
2018–2019	GLM 1 Sub-Epidemic	5609.4	4838.5	185222	6.7%
	GLM 2 Sub-Epidemics	2974.4	2458.5	89619	6.7%
	GLM 3 Sub-Epidemics	2118.6	1569.9	53515	6.7%

4.4 2015–2016 Season Results

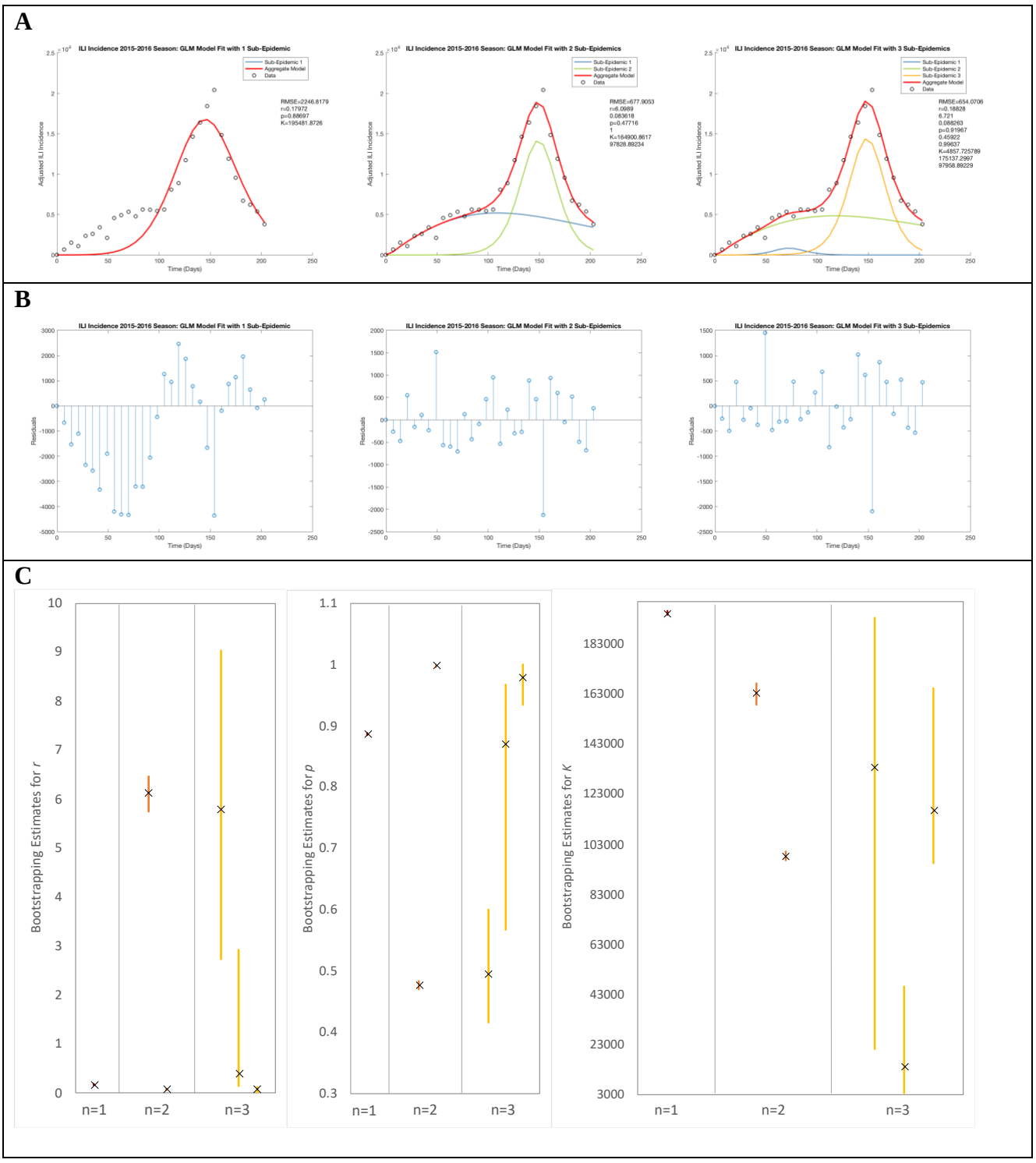

Figure 7 2015–2016 results. A) Sub-epidemic curves generated by fitting the model with 1, 2, and 3 sub-epidemics (L to R). The red line is the aggregate curve. B) Residuals from model fit to epidemic period data, sub-epidemics 1, 2, and 3 (L to R). C) Parameter estimates (marked by *x*) and 95% confidence intervals generated by bootstrap method using 200 simulated datasets. First chart shows *r*, sub-epidemics 1, 2, and 3, followed by similar charts for *p* and *K*.

4.5 2016–2017 Season Results

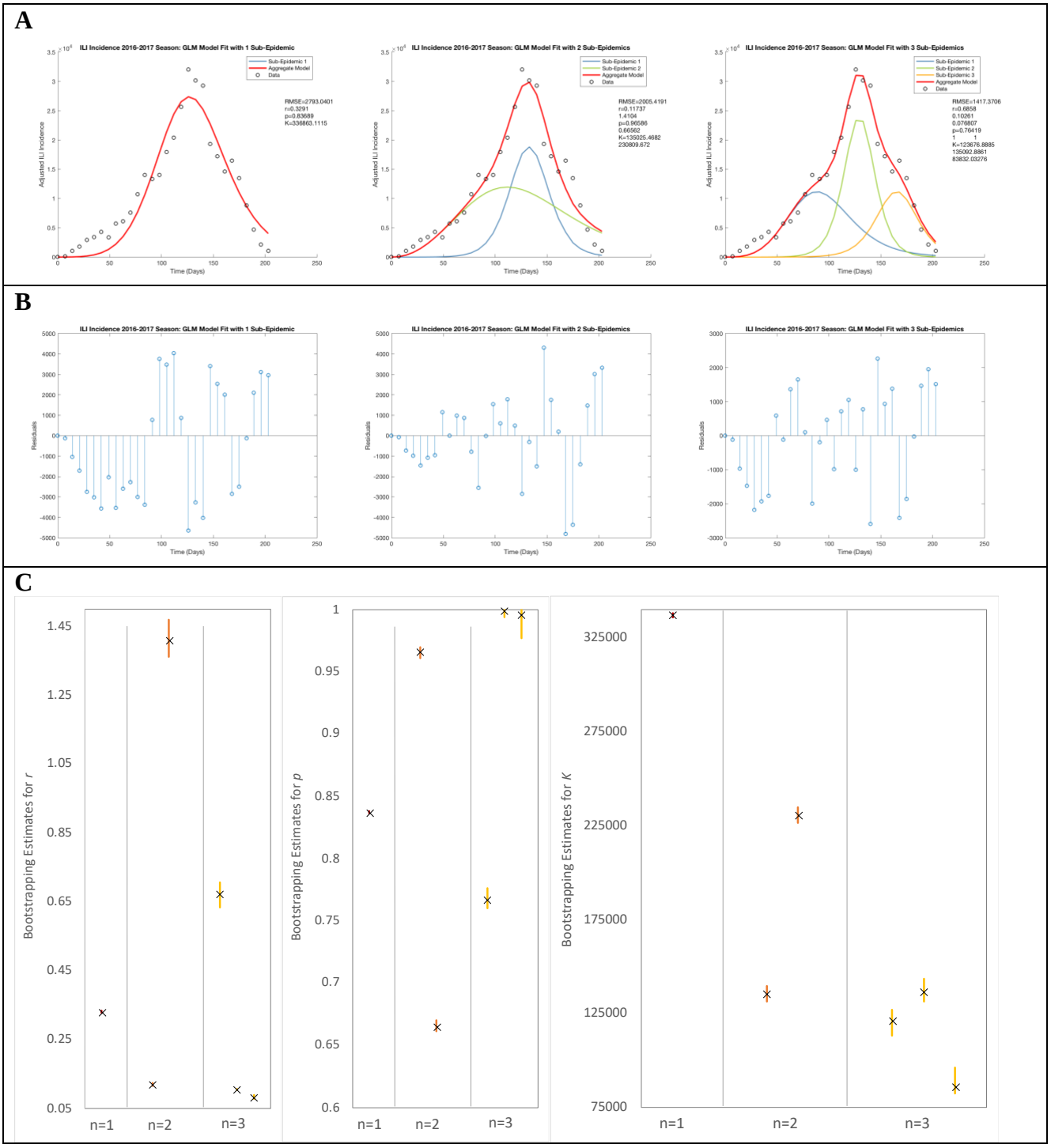

Figure 8 2016–2017 results. A) Sub-epidemic curves generated by fitting the model with 1, 2, and 3 sub-epidemics (L to R). The red line is the aggregate curve. B) Residuals from model fit to epidemic period data, sub-epidemics 1, 2, and 3 (L to R). C) Parameter estimates (marked by *x*) and 95% confidence intervals generated by bootstrap method using 200 simulated datasets. First chart shows *r*, sub-epidemics 1, 2, and 3, followed by similar charts for *p* and *K*.

4.6 2017–2018 Season Results

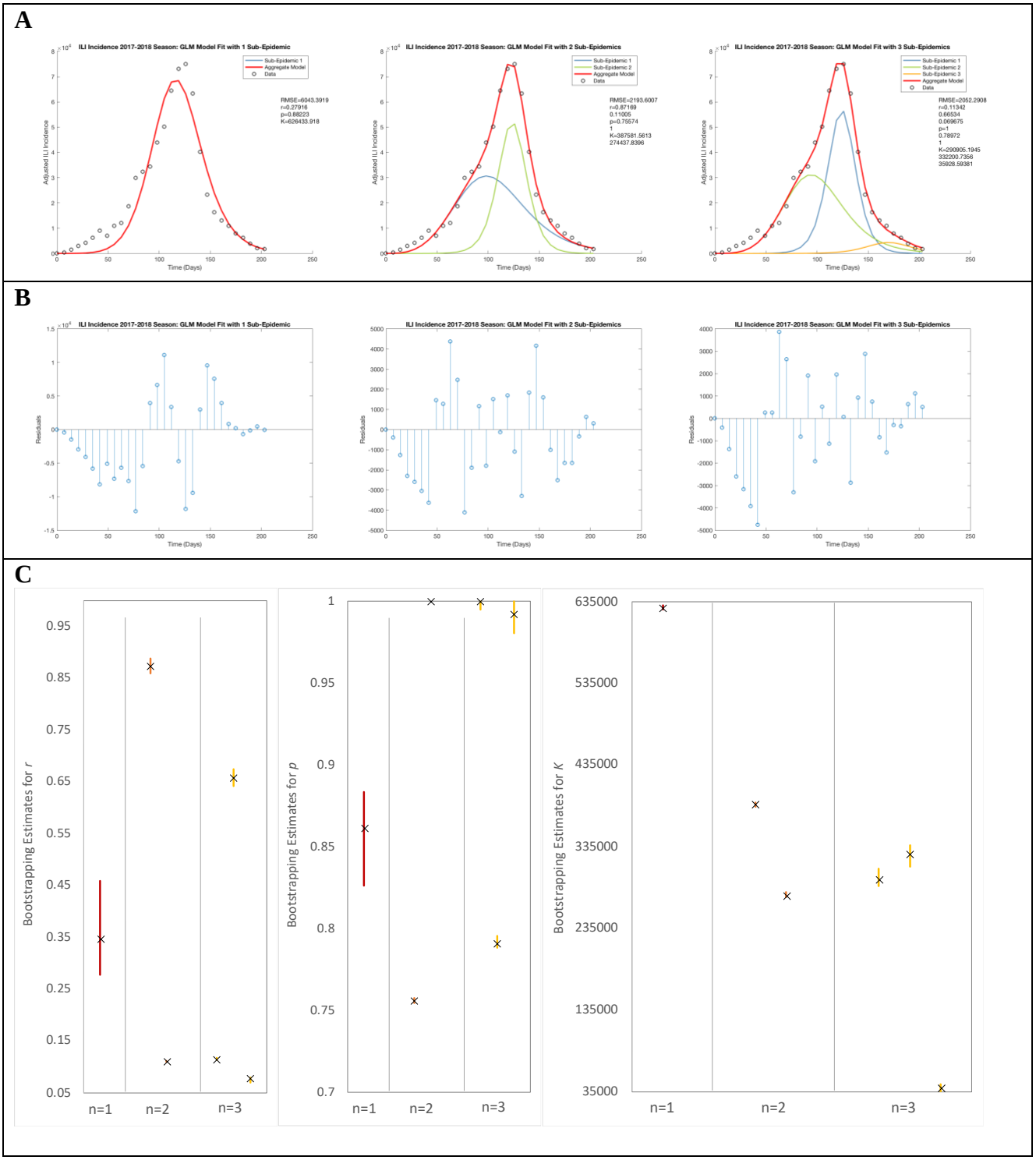

Figure 9 2017–2018 results. A) Sub-epidemic curves generated by fitting the model with 1, 2, and 3 sub-epidemics (L to R). The red line is the aggregate curve. B) Residuals from model fit to epidemic period data, sub-epidemics 1, 2, and 3 (L to R). C) Parameter estimates (marked by *x*) and 95% confidence intervals generated by bootstrap method using 200 simulated datasets. First chart shows *r*, sub-epidemics 1, 2, and 3, followed by similar charts for *p* and *K*.

4.7 2018–2019 Season Results

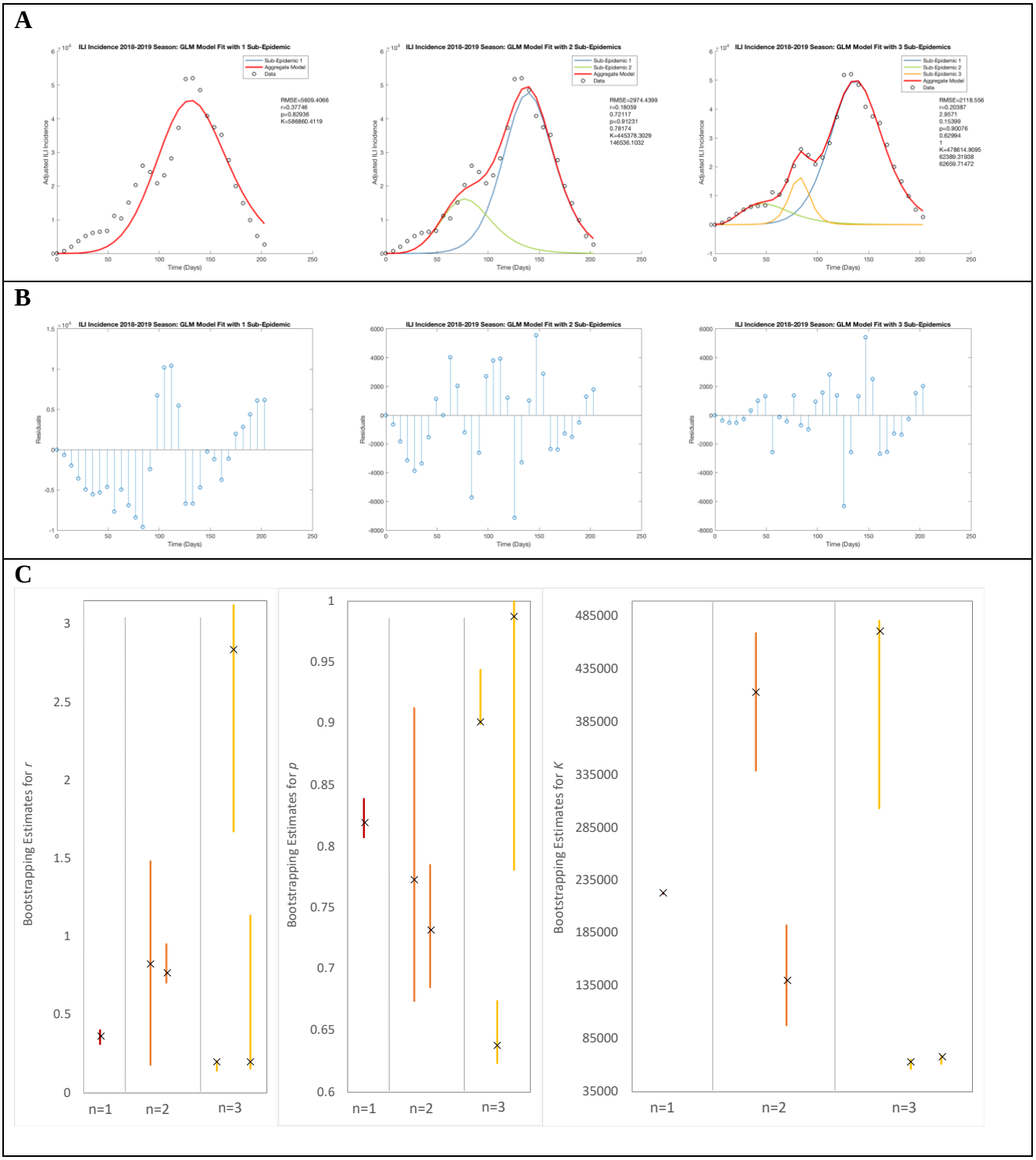

Figure 10 2018–2019 results. A) Sub-epidemic curves generated by fitting the model with 1, 2, and 3 sub-epidemics (L to R). The red line is the aggregate curve. B) Residuals from model fit to epidemic period data, sub-epidemics 1, 2, and 3 (L to R). C) Parameter estimates (marked by *x*) and 95% confidence intervals generated by bootstrap method using 200 simulated datasets. First chart shows *r*, sub-epidemics 1, 2, and 3, followed by similar charts for *p* and *K*.

4.8 Comparison to Virologic Surveillance

Model results were generated by fitting to adjusted ILI incidence data. Because ILI is nonspecific, a comparison was made to the virologic surveillance data reported by public health laboratories during the same time period. Counts and type of influenza-positive viral specimens was obtained from FluView and grouped as A (H3), A (H1N1), A (No Subtyping Done), and B (All Types). Selected results are displayed in Figure 11 with additional results included in the Appendix.

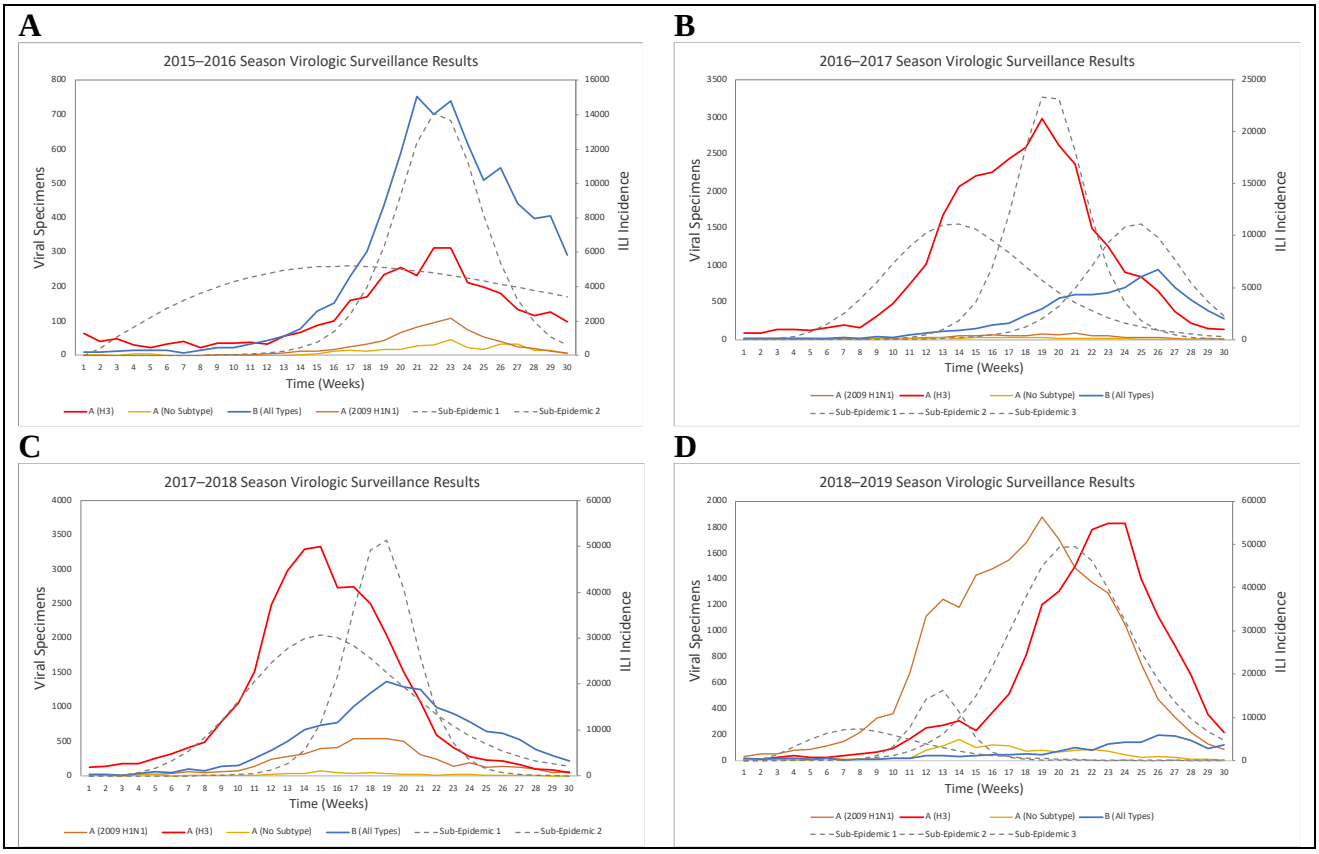

Figure 11 Counts and types of viral specimens reported to CDC each week from public health laboratories. The best fit sub-epidemic model results obtained from fitting to the adjusted ILI incidence data are shown in grey. One model from each year was selected for the figure, depending on which was most aligned to the virologic data. A) 2015–2016 season, 2 sub-epidemic model. B) 2016–2017 season, 3 sub-epidemic model. C) 2017–2018 season, 2 sub-epidemic model. D) 2018–2019 season, 3 sub-epidemic model.

CHAPTER V – DISCUSSION AND CONCLUSIONS

5.1 Discussion of Key Findings

There was a demonstrated improvement in model performance when sub-epidemics were incorporated into the GLM. As the number of sub-epidemics increased from 1 to 3, the distance between the aggregate model curve and the underlying incidence data decreased. The observed improvement in model fit is likely because the sub-epidemic model has more parameters than the 1 curve GLM and is therefore able to capture more variation in the data. This is one of the benefits of using the sub-epidemic model for influenza, as factors such as different virus types, seasonal effects, and changing vaccination coverage, can easily cause variation in the shape of the incidence curve. While the improvement in model performance is notable, improved fit does not necessarily indicate epidemiologic information has been gained. Thus, an additional benefit of the sub-epidemic model is its ability to identify and visualize complex epidemic growth dynamics from simple case count data. While the sub-epidemic curves were not always able to be traced back to an underlying epidemiologic cause, several results from this investigation support the conclusion that incorporation of 2 or 3 sub-epidemics into the model enhanced identification of unique seasonal characteristics.

The 2015–2016 season peaked in mid-March, which happened only two other times in the previous 18 influenza seasons (Davlin et al., 2016). While the GLM with n=1 was not able to capture both the longer left tail and the peak of the season, the GLM with n=2 and n=3 fit sub-epidemic curves to both components. The comparison of the model to the virologic data indicates that the left tail observed in the ILI data for this season may not have been caused by influenza, due to the absence of reported viral specimens during that time (Figure 11A). Instead, this feature was likely a result of using standard season start and end dates that were not specific

enough for each year. However, despite the inclusion of ILI noise at the start of this season, the sub-epidemic model separated that component out into its own sub-epidemic. This is helpful because it was able to fit the left tail and peak separately, which helps to limit the effects of ILI noise on parameter estimation for peak growth dynamics.

Comparison of the virologic surveillance data to the 3 sub-epidemic model for the 2016–2017 season showed that the model was able to successfully identify individual peaks for A (H3) viruses and B viruses (Figure 11B). This season primarily consisted of influenza A (H3N2) viruses, but a small wave of influenza B activity was seen late in the season, from the end of March through May (Blanton et al., 2017). The model identified a small sub-epidemic curve later in the season, which aligned with the timing of the emergence of the influenza B virus wave. In addition, for this season, the narrow confidence interval around each parameter estimate supports the identifiability of the results, even with 9 parameters being estimated from the data. Similar results were seen for the 2017–2018 season, where both sub-epidemics from the 2 sub-epidemic model aligned with peak timing for two waves seen in the viral results: an initial influenza A (H3N2) virus wave followed by an influenza B wave (Figure 11C) (Garten et al., 2018).

The 2018–2019 influenza season was also characterized by two waves of activity, however both due to influenza A viruses. During this season, there was an initial wave of influenza A (H1N1), followed by a second wave of influenza A (H3N2) viruses (Xu et al., 2019). The 2 and 3 sub-epidemic models did not distinguish the two waves, instead combining both into one large sub-epidemic (Figure 11D). This is likely because the ILI incidence was not able to capture the distinction between the two waves, since the peaks of both waves were relatively close, separated by 7 weeks, and of similar magnitude. The similarities in growth patterns between the two waves mean the curves would share transmission dynamics and similar

parameter estimates. It is possible that the sub-epidemic curves indicate another component of transmission, such as variation due to different spread among age groups or across different regions. However, a brief analysis of the curve stratified by age group and HHS regions components did not show any notable differences from the overall ILI incidence curve. Although the model combined the two viral activity waves into one, Figure 10C shows wide 95% CIs around the parameter estimates for *r*, *p*, and *K*, indicating uncertainty. The uncertainty around estimates for this season is much higher than the uncertainty for the 3 sub-epidemic model for the two previous seasons. Thus, this finding supports the continued use of parameter identifiability metrics, as these metrics provided crucial information about the certainty of the model results. For both seasons where the models did not align closely with virologic surveillance, 2015–2016 and 2018–2019, uncertainty around the parameters was much higher than for the other two seasons that were aligned with activity waves observed in the virologic surveillance.

5.2 Strengths and Limitations

This investigation used national ILI surveillance data to validate the use of the sub-epidemic GLM, which was a novel framework introduced by Chowell and Tariq in 2019. One of the strengths of the model is that it is built on assumptions about exponential growth and can be applied to different diseases, periods of time, and regions. In addition, the results demonstrated the ability of the model to identify meaningful information about complex growth dynamics from simple data, which is notable considering the challenges surrounding collection, use, and validation of surveillance data. Overall, the model was scalable, easily modified, and provided results quickly once the programming was set up.

Another strength of the investigation was that the methodology for measuring uncertainty was able to identify the two seasons that did not align with underlying virologic transmission dynamics. Measures of model fit, such as RMSE and MAE, were not by themselves sufficient to identify this, but the parameter identifiability metrics obtained through bootstrapping provided another tool for evaluation. Overall, the process developed for fitting and evaluating the model, including the least squares curve-fitting and bootstrapping, were shown to be comprehensive and necessary.

In practice, there is a need to obtain results in real time, which means the full shape of the epidemic curve is not going to be available. It would be beneficial to further investigate the accuracy of the sub-epidemic model when applied to the early growth period of the influenza season. Preliminary results were explored during this investigation by applying the methodology to the early growth period of the 2018–2019 season. The sub-epidemic model fit and bootstrapping process was repeated on a series of seven time periods with an increasing number of data points, starting at 6 data points and sequentially increasing until 12 data points. The preliminary results showed that model fit to the early growth period was also improved by incoporating sub-epidemics into the GLM. However, more thorough investigation is needed to understand how the model performs with a number of data points fewer than 30.

One of the limitations of the investigation was the nonspecific definition of epidemic periods, which added noise into the data. The start and end periods were standardly defined for consistency and to control factors that might affect model comparison. Further development of the methodology around how to precisely determine the epidemic threshold is needed to improve the results. Suggestions in the literature include use of a baseline (Xu et al. 2019; WHO, 2015),

identification of monotonic increases (Viboud, Simonsen & Chowell, 2016), or use of an algorithm such as the Nelder-Mead simplex algorithm (Charu et al., 2017).

Finally, more investigation is needed to understand how to translate the information gained from modeling ILI counts for application to influenza dynamics. Since the influenza surveillance system into the U.S. monitors several components to understand influenza activity, it would be valuable to see how other types of influenza surveillance data could contribute to the model process and whether or not other data sources are more appropriate.

5.3 Conclusion

There is value in the use and validation of phenomenological and parsimonious models that can quickly generate meaningful results on simple epidemic curve data. The GLM, in all of its forms, generated meaningful results when applied to a period of epidemic growth for seasonal influenza. Incorporating sub-epidemics (n=2 or n=3) into the GLM improved model performance and fit. Most significantly, the sub-epidemic model identified unique characteristics of each season that were not immediately observable from the aggregate epidemic curve. For two of the four seasons investigated, model sub-epidemics were aligned with underlying virologic transmission trends. For the two seasons that were not aligned with virologic results, the methodology for determining uncertainty around parameter estimates indicated relatively high uncertainty. These findings support the continued use of this model for academic and other public health application.

REFERENCES

Baltrusaitis, K., Vespignani, A., Rosenfeld, R., Gray, J., Raymond, D., & Santillana, M. (2019). Differences in Regional Patterns of Influenza Activity Across Surveillance Systems in the United States: Comparative Evaluation. *JMIR public health and surveillance*, *5*(4), e13403. https://doi.org/10.2196/13403

Barnston, A. (1992). Correspondence among the correlation, RMSE, and Heidke forecast verification measures; refinement of the Heidke score. *Weather and Forecasting*, *7*(4), 699-709. https://doi.org/10.1175/1520-0434(1992)007%3C0699:CATCRA%3E2.0.CO;2

Barr, I. G., & Cheng, A. C. (2018). Difficulties of predicting the timing, size and severity of influenza seasons. *Respirology*, *23*(6), 562–563. https://doi.org/10.1111/resp.13310

Bensimon, C. M., & Upshur, R. E. G. (2007). Evidence and effectiveness in decisionmaking for quarantine. *American Journal of Public Health*, *97 Suppl 1*, 44–48. https://doi.org/10.2105/AJPH.2005.077305

Bertozzi, A.L., Franco, E., Mohler, G., Short, M.B., Sledge, D. (2020). The challenges of modeling and forecasting the spread of COVID-19. *Proceedings of the National Academy of Sciences, 117*(29), 16732-16738. doi:10.1073/pnas.2006520117

Biggerstaff, M., Dahlgren, F. S., Fitzner, J., George, D., Hammond, A., Hall, I., … Wu, J. T. (2019). Coordinating the real-time use of global influenza activity data for better public health planning. *Influenza and Other Respiratory Viruses*. https://doi.org/10.1111/irv.12705

Blanton, L., Alabi, N., Mustaquim, D., Taylor, C., Kniss, K., Kramer, N., Budd, A., Garg, S., Cummings, C. N., Chung, J., Flannery, B., Fry, A. M., Sessions, W., Garten, R., Xu, X., Elal, A. I. A., Gubareva, L., Barnes, J., Dugan, V., … Brammer, L. (2017). Update: Influenza Activity in the United States During the 2016–17 Season and Composition of the 2017–18 Influenza Vaccine. *MMWR. Morbidity and Mortality Weekly Report*, *66*(25), 668–676. https://doi.org/10.15585/mmwr.mm6625a3

Brockmann, D, & Helbing, D. (2013). The hidden geometry of complex, network-driven contagion phenomena. *Science, 342*(6164), 1337–1342. https://doi.org/10.1126/science.1245200

Casals, M., Girabent-Farrés, M., & Carrasco, J. L. (2014). Methodological Quality and Reporting of Generalized Linear Mixed Models in Clinical Medicine (2000–2012): A Systematic Review. *PLoS ONE*, *9*(11), 1–10. https://doi.org/10.1371/journal.pone.0112653

Centers for Disease Control and Prevention (CDC). Principles of epidemiology in public health practice. 3rd ed. Centers for Disease Control and Prevention; 2011. https://www.cdc.gov/csels/dsepd/ss1978/lesson1/section6.html. Accessed April 24, 2020.

Centers for Disease Control and Prevention (CDC). (n.d.). *Weeks ending log 2017–2018* [PDF file]. Retrieved from https://wwwn.cdc.gov/nndss/document/w2017-18.pdf

Charu, V., Zeger, S., Gog, J., Bjørnstad, O. N., Kissler, S., Simonsen, L., Grenfell, B. T., & Viboud, C. (2017). Human mobility and the spatial transmission of influenza in the United States. *PLoS Computational Biology*, *13*(2), 1–23. https://doi.org/10.1371/journal.pcbi.1005382

Chowell, G., Hincapie-Palacio, D., Ospina, J., Pell, B., Tariq, A., Dahal, S., Moghadas, S., Smirnova, A., Simonsen, L., & Viboud, C. (2016a). Using Phenomenological Models to Characterize Transmissibility and Forecast Patterns and Final Burden of Zika Epidemics. *PLoS Currents*, *3*, 1–16. https://doi.org/10.1371/currents.outbreaks.f14b2217c902f453d9320a43a35b9583

Chowell, G., Sattenspiel, L., Bansal, S., & Viboud, C. (2016b). Mathematical models to characterize early epidemic growth: A review. *Physics of life reviews*, *18*, 66–97. https://doi.org/10.1016/j.plrev.2016.07.005

Chowell, G., Tariq, A., & Hyman, J. M. (2019). A novel sub-epidemic modeling framework for short-term forecasting epidemic waves. *BMC Medicine*, *17*(1), 1–18. https://doi.org/10.1186/s12916-019-1406-6

Davlin, S. L., Blanton, L., Kniss, K., Mustaquim, D., Smith, S., Kramer, N., Cohen, J., Cummings, C. N., Garg, S., Flannery, B., Fry, A. M., Grohskopf, L. A., Bresee, J., Wallis, T., Sessions, W., Garten, R., Xu, X., Elal, A. I. A., Gubareva, L., … Brammer, L. (2016). Influenza Activity — United States, 2015–16 Season and Composition of the 2016–17 Influenza Vaccine. *MMWR. Morbidity and Mortality Weekly Report*, *65*(22), 567–575. https://doi.org/10.15585/mmwr.mm6522a3

de Picoli Junior, S., Teixeira, J. J., Ribeiro, H. V., Malacarne, L. C., dos Santos, R. P., & dos Santos Mendes, R. (2011). Spreading patterns of the influenza A (H1N1) pandemic. *PloS one*, *6*(3), e17823. https://doi.org/10.1371/journal.pone.0017823

Fischer, A. J., & Ghelardi, G. (2016). The Precautionary Principle, Evidence-Based Medicine, and Decision Theory in Public Health Evaluation. *Frontiers in public health*, *4*, 107. https://doi.org/10.3389/fpubh.2016.00107

Garcia, M. C., Garrett, N. Y., Singletary, V., Brown, S., Hennessy-Burt, T., Haney, G., Link, K., Tripp, J., Mac Kenzie, W. R., & Yoon, P. (2018). An Assessment of Information Exchange Practices, Challenges, and Opportunities to Support US Disease Surveillance in 3 States. *Journal of public health management and practice : JPHMP*, *24*(6), 546–553. https://doi.org/10.1097/PHH.0000000000000625

Garten, R., Blanton, L., Isa, A., Elal, A., Alabi, N., Barnes, J., Biggerstaff, M., Brammer, L., Budd, A. P., Burns, E., Cummings, C. N., Davis, T., Garg, S., Gubareva, L., Jang, Y.,

Kniss, K., Kramer, N., Lindstrom, S., Mustaquim, D., … Jernigan, D. (2018). *Update : Influenza Activity in the United States During the 2017 – 18 Season and Composition of the 2018 – 19 Influenza Vaccine Antigenic and Genetic Characterization of Influenza Viruses*. *67*(22).

Goh, K. T., Cutter, J., Heng, B. H., Ma, S., Koh, B. K. W., Kwok, C., … Chew, S. K. (2006). Epidemiology and control of SARS in Singapore. *Annals of the Academy of Medicine Singapore*, *35*(5), 301–316.

Goldstein, B. D. (2012). John Snow, the Broad Street pump and the precautionary principle. *Environmental Development*, *1*(1), 3–9. https://doi.org/10.1016/j.envdev.2011.12.002

Harremoes, P., Gee, D., MacGarvin, M., Stirling, A., Keys, J., Wynne, B., & Guedes Vaz, S. (2002). *The Precautionary Principle in the 20th Century : Late Lessons From Early Warnings*. Routledge.

Hunt, A. G. (2014). Exponential Growth in Ebola Outbreak Since May 14, 2014. *Complexity*, *20*(2), 8–11. https://doi.org/10.1002/cplx.21615

Kegge, R. (2020). The precautionary principle and the burden and standard of proof in European and Dutch environmental law. *Review of European Administrative Law*, *13*(2), 113–121. https://doi.org/10.7590/187479820X159307018522741874-7981

Lipsitch, M., Cohen, T., Cooper, B., Robins, J. M., Ma, S., James, L., … Murray, M. (2003). Transmission dynamics and control of severe acute respiratory syndrome. *Science*, *300*(5627), 1966–1970. https://doi.org/10.1126/science.1086616

Lofgren, E., Fefferman, N. H., Naumov, Y. N., Gorski, J., & Naumova, E. N. (2007). Influenza Seasonality: Underlying Causes and Modeling Theories. *Journal of Virology*, *81*(11), 5429–5436. https://doi.org/10.1128/jvi.01680-06

Lowen, A. C., Mubareka, S., Steel, J., & Palese, P. (2007). Influenza virus transmission is dependent on relative humidity and temperature. *PLoS Pathogens*, *3*(10), 1470–1476. https://doi.org/10.1371/journal.ppat.0030151

Leuba, S. I., Yaesoubi, R., Antillon, M., Cohen, T., & Zimmer, C. (2020). Tracking and predicting U.S. influenza activity with a real-time surveillance network. *PLoS Computational Biology*, *16*(11), 1–14. https://doi.org/10.1371/journal.pcbi.1008180

Maier, B. F., & Brockmann, D. (2020). Effective containment explains sub-exponential growth in confirmed cases of recent COVID-19 outbreak in Mainland China. *ArXiv*, *746*(May), 742–746. https://doi.org/10.1101/2020.02.18.20024414

Martuzzi, M., & Tickner, J. a. (2004). The precautionary principle: protecting public health, the environment and the future of our children. *World Health Organisation*, 220. Retrieved from http://www.euro.who.int/__data/assets/pdf_file/0003/91173/E83079.pdf

Matrajt, L., & Leung, T. (2020). Evaluating the Effectiveness of Social Distancing Interventions to Delay or Flatten the Epidemic Curve of Coronavirus Disease. *Emerging Infectious Diseases*, *26*(8), 1740–1748. https://doi.org/10.3201/eid2608.201093

Murphy, M. S. Q., Wilson, K., Atkinson, K. M., Fergusson, D. A., Forster, A., Tinmouth, A. T., Brown, A., & Keelan, J. (2019). Problems with precaution: the transfusion medicine experience. *Journal of Risk Research*, *22*(2), 137–149. https://doi.org/10.1080/13669877.2017.1351478

Nasserie, T., Tuite, A. R., Whitmore, L., Hatchette, T., Drews, S. J., Peci, A., Kwong, J. C., Friedman, D., Garber, G., Gubbay, J., & Fisman, D. N. (2017). Seasonal Influenza Forecasting in Real Time Using the Incidence Decay With Exponential Adjustment Model. *Open Forum Infectious Diseases*, *4*(3). https://doi.org/10.1093/ofid/ofx166

National Center for Immunization and Respiratory Diseases (CDC NCIRD). (2020a, October 6). *U.S. influenza surveillance system: purpose and methods*. https://www.cdc.gov/flu/weekly/overview.htm

National Center for Immunization and Respiratory Diseases (CDC NCIRD). (2020b, January 8). *Estimated influenza illnesses, medical visits, hospitalizations, and deaths in the United States — 2018–2019 influenza season*. https://www.cdc.gov/flu/about/burden/2018-2019.html

Paul, S., Mgbere, O., Arafat, R., Yang, B., & Santos, E. (2017). Modeling and Forecasting Influenza-like Illness (ILI) in Houston, Texas Using Three Surveillance Data Capture Mechanisms. *Online journal of public health informatics*, *9*(2), e187. https://doi.org/10.5210/ojphi.v9i2.8004

Roosa, K., & Chowell, G. (2019). Assessing parameter identifiability in compartmental dynamic models using a computational approach: application to infectious disease transmission models. *Theoretical Biology and Medical Modelling*, *16*(1), 1–15. https://doi.org/10.1186/s12976-018-0097-6

Sah, P., Alfaro-Murillo, J. A., Fitzpatrick, M. C., Neuzil, K. M., Meyers, L. A., Singer, B. H., & Galvani, A. P. (2019). Future epidemiological and economic impacts of universal influenza vaccines. *Proceedings of the National Academy of Sciences of the United States of America*, *116*(41), 20786–20792. https://doi.org/10.1073/pnas.1909613116

Strong, P. (1990). Epidemic psychology: a model. *Sociology of Health & Illness*, *12*(3), 249–259. https://onlinelibrary.wiley.com/doi/pdf/10.1111/1467-9566.ep11347150

Tamerius J, Steadman J, Tamerius J. Synchronicity of influenza activity within Phoenix, AZ during the 2015-2016 seasonal epidemic. *BMC Infectious Diseases*. 2017;17(1):109. doi:10.1186/s12879-017-2197-z.

Vandekerckhove, J., Matzke, D., & Wagenmakers, E.-J. (2015). *Model comparison and the principle of parsimony.* In J. R. Busemeyer, Z. Wang, J. T. Townsend, & A. Eidels (Eds.), *Oxford library of psychology. The Oxford handbook of computational and mathematical psychology* (p. 300–319). Oxford University Press.

Verity, R., Okell, L. C., Dorigatti, I., Winskill, P., Whittaker, C., Imai, N., Cuomo-Dannenburg, G., Thompson, H., Walker, P., Fu, H., Dighe, A., Griffin, J. T., Baguelin, M., Bhatia, S., Boonyasiri, A., Cori, A., Cucunubá, Z., FitzJohn, R., Gaythorpe, K., Green, W., … Ferguson, N. M. (2020). Estimates of the severity of coronavirus disease 2019: a model-based analysis. *The Lancet. Infectious diseases*, *20*(6), 669–677.

Viboud, C., Simonsen, L., & Chowell, G. (2016). A generalized-growth model to characterize the early ascending phase of infectious disease outbreaks. *Epidemics*, *15*, 27–37. https://doi.org/10.1016/j.epidem.2016.01.002

Vynnycky, E., & White, R. (2010). *Introduction to infectious disease modelling*. Oxford: Oxford University Press.

Waldner, C., Osgood, N., & Seitzinger, P. (2017). Big data for infectious diseases surveillance and the potential contribution to the investigation of foodborne disease in Canada. *National Collaborative Centre for Infectious Diseases Canada*. https://nccid.ca/publications/big-data-for-infectious-diseases-surveillance/

Willmott, C. J., & Matsuura, K. (2005). Advantages of the mean absolute error (MAE) over the root mean square error (RMSE) in assessing average model performance. *Climate Research*, *30*(1), 79–82. https://doi.org/10.3354/cr030079

World Health Organization. (2015). A manual for estimating disease burden associated with seasonal influenza. World Health Organization. https://apps.who.int/iris/handle/10665/178801

Xu, X., Blanton, L., Elal, A. I. A., Alabi, N., Barnes, J., Biggerstaff, M., Brammer, L., Budd, A. P., Burns, E., Cummings, C. N., Garg, S., Kondor, R., Gubareva, L., Kniss, K., Nyanseor, S., O'Halloran, A., Rolfes, M., Sessions, W., Dugan, V. G., … Jernigan, D. (2019). Update: Influenza Activity in the United States During the 2018–19 Season and Composition of the 2019–20 Influenza Vaccine. *MMWR. Morbidity and Mortality Weekly Report*, *68*(24), 544–551. https://doi.org/10.15585/mmwr.mm6824a3

APPENDIX

Table 4 Parameter estimates and confidence intervals determined from bootstrapping with 200 realizations.

Model Type	Growth Rate (r)	Growth Scaling Factor (p)	Total Epidemic Size (K)
2015–2016 SEASON			
GLM 1 Sub-Epidemic	r: 0.180 (0.178, 0.182)	p: 0.887 (0.885, 0.889)	K: 195,496 (194689, 196369)
GLM 2 Sub-Epidemics	r_1: 6.13 (5.75, 6.47)	p_1: 0.477 (0.471, 0.484)	K_1: 163,841 (159063, 167677)
	r_2: 0.0840 (0.0835, 0.0853)	p_2: 1.00 (0.996, 1.00)	K_2: 98,335 (96856, 100106)
GLM 3 Sub-Epidemics	r_1: 5.81 (2.74, 9.04)	p_1: 0.495 (0.416, 0.601)	K_1: 134,163 (21407, 193744)
	r_2: 0.415 (0.153, 2.93)	p_2: 0.871 (0.567, 0.967)	K_2: 14,541 (3588, 46295)
	r_3: 0.0100 (0.0864, 0.131)	p_3: 0.979 (0.934, 1.00)	K_3: 116,813 (95696, 165513)
2016-2017 SEASON			
GLM 1 Sub-Epidemic	r: 0.329 (0.326, 0.332)	p: 0.837 (0.836, 0.838)	K: 336,897 (335785, 337988)
GLM 2 Sub-Epidemics	r_1: 0.118 (0.114, 0.122)	p_1: 0.966 (0.961, 0.970)	K_1: 135,211 (131105, 139399)
	r_2: 1.41 (1.36, 1.47)	p_2: 0.665 (0.661, 0.670)	K_2: 230,647 (226243, 234652)
GLM 3 Sub-Epidemics	r_1: 0.673 (0.632, 0.705)	p_1: 0.767 (0.760, 0.776)	K_1: 120,966 (113199, 126581)
	r_2: 0.103 (0.102, 0.106)	p_2: 0.999 (0.994, 1.00)	K_2: 136,165 (131386, 143287)
	r_3: 0.0822 (0.0765, 0.0889)	p_3: 0.996 (0.977, 1.00)	K_3: 85,684 (81967, 96185)
2017-2018 SEASON			
GLM 1 Sub-Epidemic	r: 0.347 (0.278, 0.459)	p: 0.861 (0.826, 0.883)	K: 627,748 (625015, 629841)
GLM 2 Sub-Epidemics	r_1: 0.874 (0.860, 0.888)	p_1: 0.756 (0.754, 0.757)	K_1: 386,670 (383192, 389191)
	r_2: 0.110 (0.110, 0.112)	p_2: 1.00 (1.00, 1.00)	K_2: 275,426 (272855, 279145)
GLM 3 Sub-Epidemics	r_1: 0.114 (0.113, 0.117)	p_1: 1.00 (0.995, 1.00)	K_1: 294,312 (287170, 307218)
	r_2: 0.657 (0.641, 0.675)	p_2: 0.791 (0.788, 0.795)	K_2: 325,660 (310845, 336819)
	r_3: 0.0780 (0.0692, 0.0788)	p_3: 0.992 (0.980, 1.00)	K_3: 39,205 (34288, 44255)
2018-2019 SEASON			
GLM 1 Sub-Epidemic	r: 0.362 (0.313, 0.401)	p: 0.820 (0.807, 0.839)	K: 223,449 (223449, 223450)
GLM 2 Sub-Epidemics	r_1: 0.825 (0.179, 1.48)	p_1: 0.773 (0.674, 0.913)	K_1: 413,798 (339294, 469474)
	r_2: 0.772 (0.701, 0.951)	p_2: 0.732 (0.685, 0.785)	K_2: 140,316 (97702, 192223)
GLM 3 Sub-Epidemics	r_1: 0.202 (0.139, 0.206)	p_1: 0.902 (0.900, 0.944)	K_1: 471,806 (303,216, 480983)
	r_2: 2.84 (1.67, 3.12)	p_2: 0.638 (0.623, 0.674)	K_2: 63,854 (56659, 65356)
	r_3: 0.197 (0.154, 1.13)	p_3: 0.988 (0.781, 1.00)	K_3: 68,265 (61624, 68875)

A) n=1

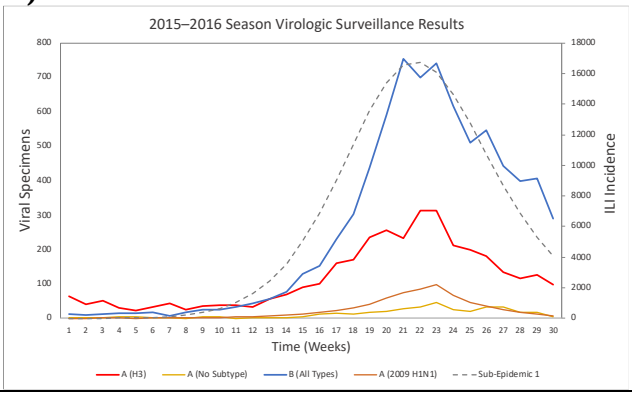

B) n=2

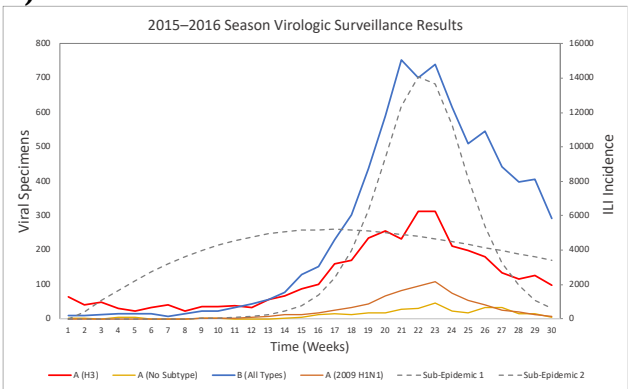

C) *n*=3

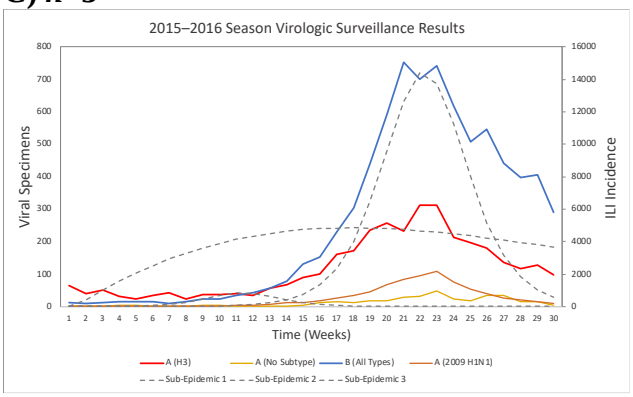

Figure 12 Results from the 2015–2016 season. The type and count of viral specimens reported from public health laboratories are shown along with the GLM sub-epidemic best fit model results obtained from fitting to the ILI adjusted incidence. A) Results from the GLM with 1 sub-epidemic. B) Results from the GLM with 2 sub-epidemics. 3) Results from the GLM with 3 sub-epidemics.

A) *n*=1

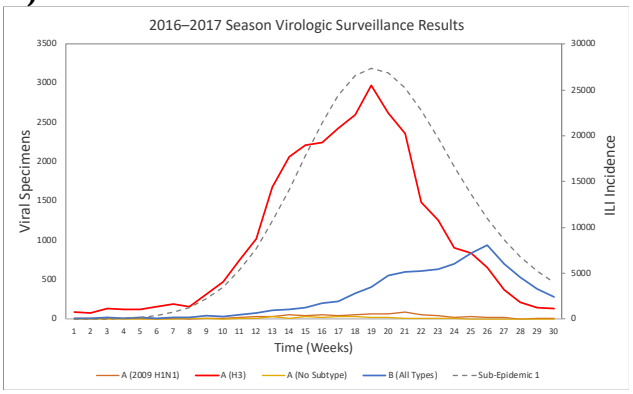

B) *n*=2

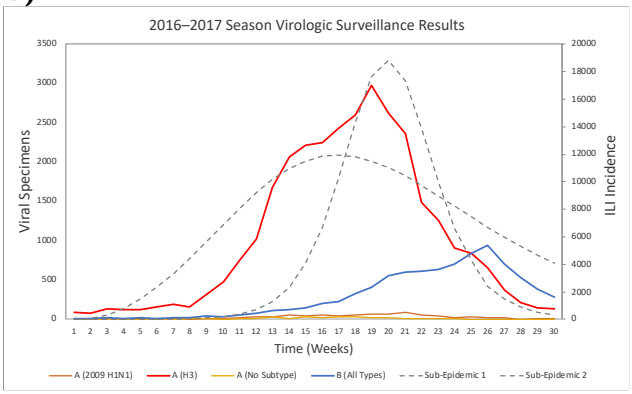

C) *n*=3

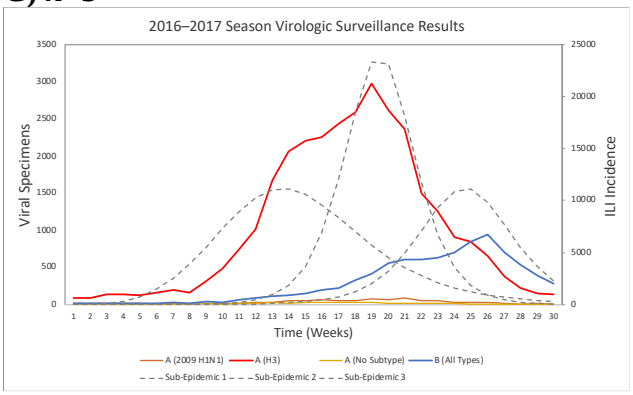

Figure 13 Results from the 2016–2017 season. The type and count of viral specimens reported from public health laboratories are shown along with the GLM sub-epidemic best fit model results obtained from fitting to the ILI adjusted incidence. A) Results from the GLM with 1 sub-epidemic. B) Results from the GLM with 2 sub-epidemics. 3) Results from the GLM with 3 sub-epidemics.

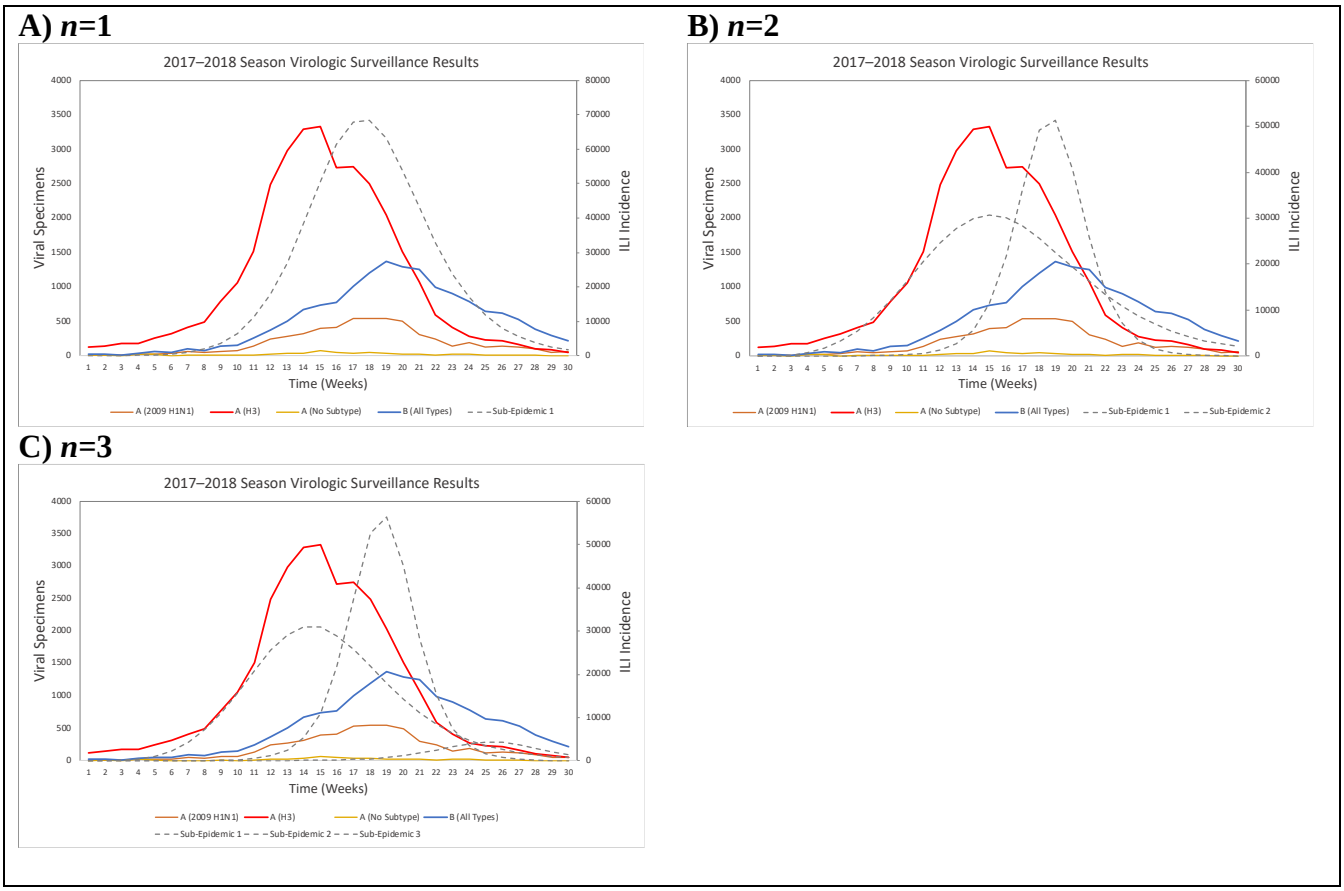

Figure 14 Results from the 2017–2018 season. The type and count of viral specimens reported from public health laboratories are shown along with the GLM sub-epidemic best fit model results obtained from fitting to the ILI adjusted incidence. A) Results from the GLM with 1 sub-epidemic. B) Results from the GLM with 2 sub-epidemics. 3) Results from the GLM with 3 sub-epidemics.

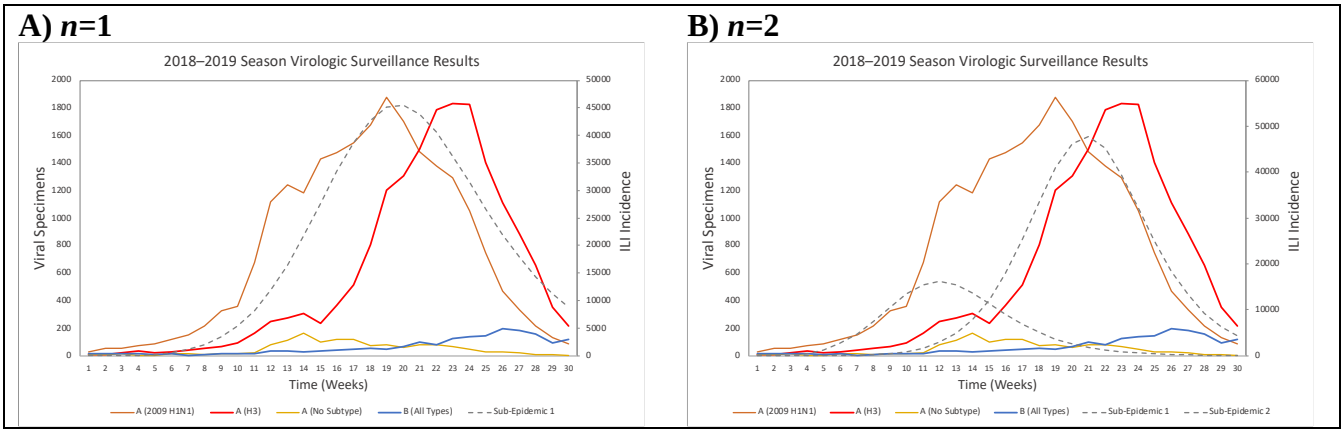

C) *n*=3

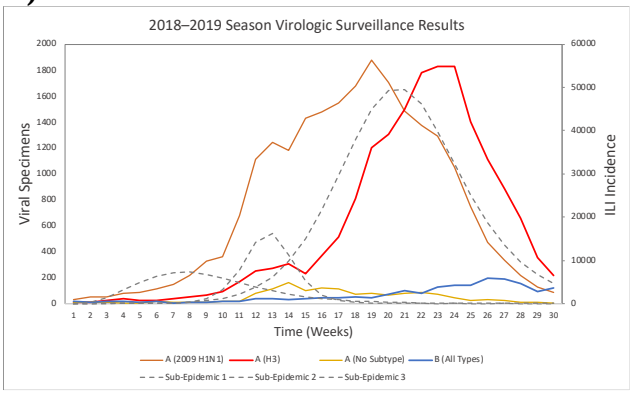

Figure 15 Results from the 2018–2019 season. The type and count of viral specimens reported from public health laboratories are shown along with the GLM sub-epidemic best fit model results obtained from fitting to the ILI adjusted incidence. A) Results from the GLM with 1 sub-epidemic. B) Results from the GLM with 2 sub-epidemics. 3) Results from the GLM with 3 sub-epidemics.